REPORT DOCUMENTATION PAGE

Form Approved OMB No. 0704-0188

1. REPORT DATE *(DD-MM-YYYY)*	2. REPORT TYPE	3. DATES COVERED *(From – To)*
24-10-2003	Final Report	3 August 2001 - 03-Aug-02

4. TITLE AND SUBTITLE

Spectrally Shaped Random-Phase Spreading Functions for Robust Wide-Bandwidth Communications

5a. CONTRACT NUMBER
F61775-01-WE042

5b. GRANT NUMBER

5c. PROGRAM ELEMENT NUMBER

6. AUTHOR(S)

Professor Richard F Ormondroyd, Vivien Comley

5d. PROJECT NUMBER

5d. TASK NUMBER

5e. WORK UNIT NUMBER

7. PERFORMING ORGANIZATION NAME(S) AND ADDRESS(ES)
Cranfield University, Royal Military College of Science
Shrivenham,
Swindon, Wiltshire SN6 8LA
United Kingdom

8. PERFORMING ORGANIZATION REPORT NUMBER
N/A

9. SPONSORING/MONITORING AGENCY NAME(S) AND ADDRESS(ES)

EOARD
PSC 802 BOX 14
FPO 09499-0014

10. SPONSOR/MONITOR'S ACRONYM(S)

11. SPONSOR/MONITOR'S REPORT NUMBER(S)
SPC 01-4042

12. DISTRIBUTION/AVAILABILITY STATEMENT

Approved for public release; distribution is unlimited.

13. SUPPLEMENTARY NOTES
Report is 50 Pages and Appendix is 18 pages in three electronic files.

14. ABSTRACT

This report results from a contract tasking Cranfield University, Royal Military College of Science as follows: The contractor will investigate application of spectrally-shaped (noise-like) random-phase spreading functions to direct-sequence spread-spectrum signals which aim to enable robust wide-bandwidth communications with enhanced low probability of intercept/low probability of detection (LPI/LPD) properties.

15. SUBJECT TERMS
EOARD, Signal Processing, Communications security, Spread Spectrum, LPI and LPD

16. SECURITY CLASSIFICATION OF:			17. LIMITATION OF ABSTRACT	18, NUMBER OF PAGES	19a. NAME OF RESPONSIBLE PERSON
a. REPORT	b. ABSTRACT	c. THIS PAGE			CHRISTOPHER E REUTER, Ph. D.
UNCLAS	UNCLAS	UNCLAS	UL	50 + 18	19b. TELEPHONE NUMBER *(Include area code)* +44 20 7514 4474

FINAL REPORT

Study funded by Wright Laboratories WPAFB Dayton, Ohio, USA.,

into

"Spectrally-Shaped Random-Phase Spreading Functions"

EOARD Contract SPC 014042

Communications and Wireless Networks Group,
Department of Aerospace, Power and Sensors,
Cranfield University, RMCS.,
Shrivenham, Swindon.
SN6 8LA, UK.

Telephone: +44 (0)1793 785260
Fax: +44 (0)1793 785902
E-mail: v.y.comley@rmcs.cranfield.ac.uk

List of contents.

Chapter 1

Introduction.

This report presents simulated and measured results for CW jammer excision in a direct sequence system, comparing a random phase spreading function with a pseudo-random binary spreading function. It also presents simulated results comparing the detection of random phase and pseudo-random spreading functions in added white Gaussian noise using delay and multiply and cyclostationary techniques. It forms the second and final report in support of EOARD contract SPC 014042.

The first report describes the baseband hardware system used to investigate CW jammer excision, and presents initial measured results.

This second report initially discusses computer simulations of the baseband system and presents results in chapter 2. The simulations are of an 'ideal' system and the levels of excision achieved are very high. This approach readily allows tests to optimise parameters such as the window function and the notch width. Chapter 3 presents further results from the baseband hardware system, extending the results of the first report by including time domain windowing. Further improvements to the hardware system include carrier modulation and autonomous channel monitoring. Chapter 4 discusses these changes and presents results.

Chapter 5 considers the problem of detecting wide-bandwidth direct sequence spread spectrum signals in poor signal to noise ratios (less than 0 dB), and compares detection probabilities for random phase and binary spreading functions using a delay and multiply detector. An alternative type of detector is presented which uses a cyclostationary approach, and comparisons for detection probability are again made between the two spreading functions.

Chapter 6 presents a discussion and conclusions drawn from the study.

The appendices contains additional graphs to those which are included in the main body of the text. A description of the various C-language software programs is also given; all of the programs being included on the CD-ROM attached to this report. The executable files are intended to be run on an IBM compatible PC running MS-DOS software or a command line window under the Windows 98 operating system.

Chapter 2

2.1 Simulated baseband adaptive system.

A block diagram of the simulated system is given in figure 1.

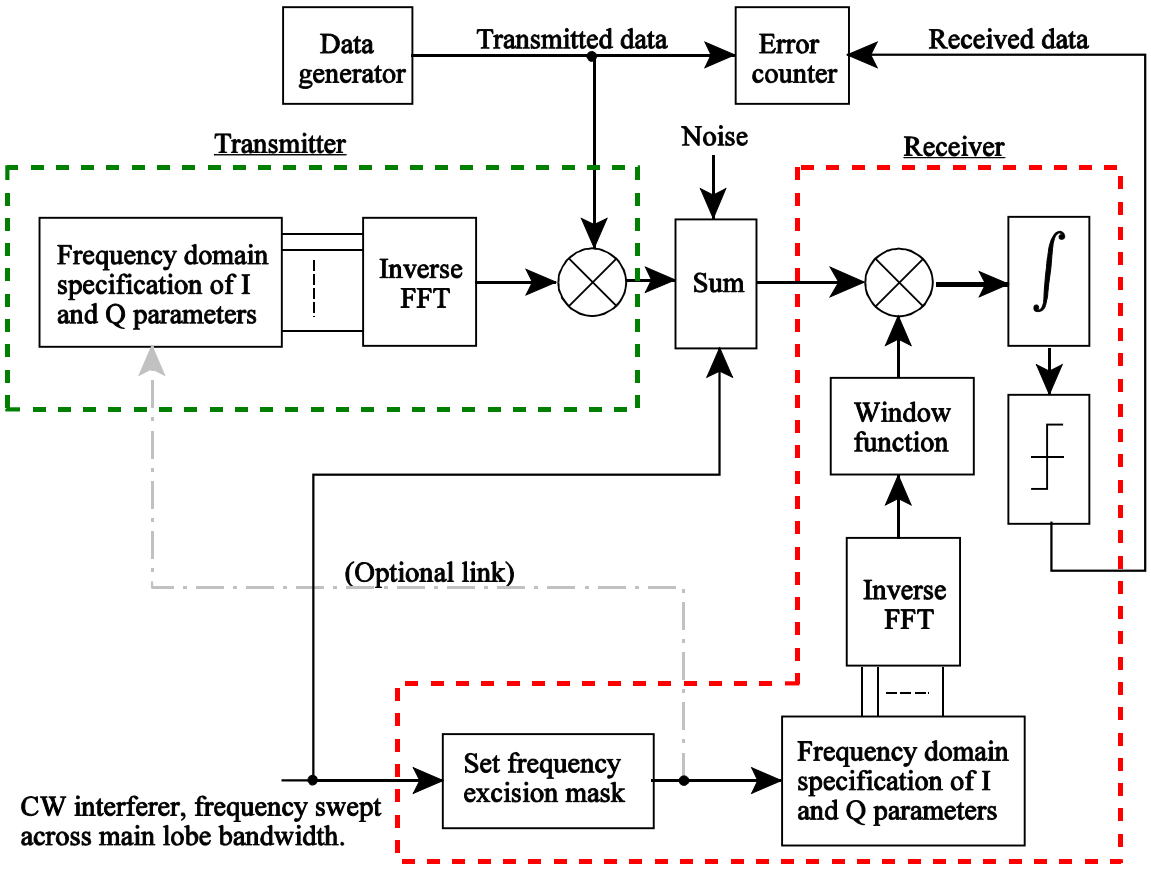

Figure 1 Block diagram of simulated adaptive DS system.

Two spreading functions were available, both being defined at the transmitter and the receiver in the frequency domain:

i) a 128-chip pseudo-random binary code band limited to the main lobe. This was formed from a 127-chip maximal length sequence padded with an extra '0' chip.

ii) an analogue noise-like function of 256 independently specified frequency bins, of which 128 bins had unity magnitude and individual random phases within the range 0 to 2π radians.

Time domain windowing, discussed in section 2.2, was used to control spectral leakage from the truncation of the high-level CW jamming signal to the Fourier transform block length at the receiver. It is convenient to apply the window to the receiver's reference function rather than at the input. Four window functions were trialed for the simulation:

i) Rectangular (no windowing),

ii) Hanning,

iii) Blackman,
iv) 4-term Blackman-Harris.

The simulations for each of the two spreading functions (binary and random phase) measured the following parameters against a swept frequency CW interferer:

a) Width of the spectral null required for optimum jammer excision.
b) Data bit error probability against added white Gaussian noise for windowed reference functions. This measures the reduction in process gain as a result of reference code windowing.
c) The advantage gained in the signal to jamming noise ratio by the frequency domain null in the reference function.

2.2 Excision null.

Both time domain functions were represented by 512 samples, hence in the frequency domain there were 256 bins which could be independently specified (figure 2). 128 bins were specified as in-phase and quadrature-phase components (pseudo-noise function) or unity amplitude and random phase (random phase function), the remaining 128 being set to zero amplitude. The highest frequency component of both time domain functions was therefore represented by 4 samples per cycle.

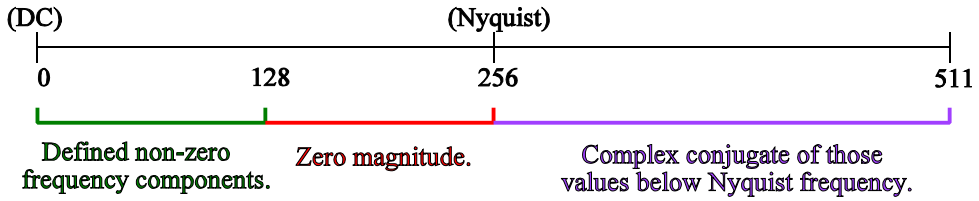

Figure 2 Frequency components of spreading and despreading functions.

Placing a spectral null within the receiver's reference function at the frequency of the narrow band interferer will reduce the interference power within the despread bandwidth, but will also reduce the process gain and hence the recovered signal to noise power ratio when additive white Gaussian noise is present. It is therefore important to ensure that the width of the spectral null is minimised, consistent with the requirement to achieve effective excision of the narrow band interferer.

If the transmitted spreading function has spectral nulls inserted which are identical to the receiver's reference function, whilst maintaining the total transmitted power constant by proportionally increasing the power in the remaining bins, the recovered signal power and demodulated bit error probability will remain constant as the null width increases. This would require a feedback channel from the receiver to the transmitter but would not normally be a practical option and has not been considered in these tests.

The despread correlator within the receiver consists of a multiplier (double balanced modulator) and an integrate and dump filter.

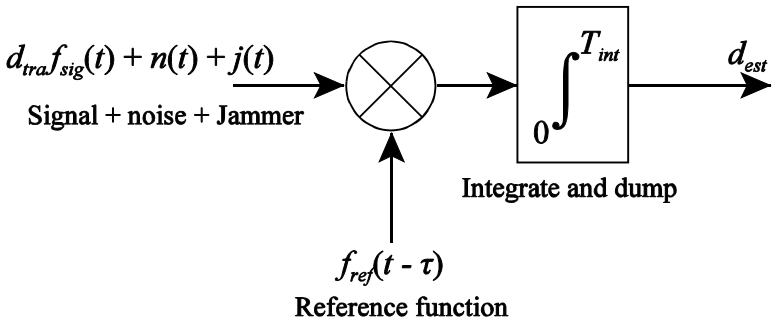

Figure 3 Despread correlator within the receiver.

The output from the integrator at the end of the integration period, d_{est}, used as an estimate of the received data symbol, is given by:

$$d_{est} = \int_0^{T_{\text{int}}} \{f_{ref}(t-\tau) \cdot [d_{tra} \cdot f_{sig}(t) + n(t) + j(t)]\} dt$$

Where $f_{ref}(t - \tau)$ is the receiver's wide band reference function,
d_{tra} is the transmitted data bit (±1),
$f_{sig}(t)$ is the transmitted wide band function,
$n(t)$ is added white Gaussian noise.
$j(t)$ is the CW interferer,

τ represents the phase offset between the reference and received functions. For perfect phase synchronisation (assumed), $\tau = 0$. Separating the terms:

$$d_{est} = \int_0^{T_{\text{int}}} \{d_{tra} \cdot f_{ref}(t) \cdot f_{sig}(t)\} dt + \int_0^{T_{\text{int}}} \{f_{ref}(t) \cdot n(t)\} dt + \int_0^{T_{\text{int}}} \{f_{ref}(t) \cdot j(t)\} dt$$

The first term represents the wanted data d_{tra}, as $\int_0^{T_{\text{int}}} \{f_{ref}(t) \cdot f_{sig}(t)\} dt$ is a constant term, the amplitude of which represents the peak of the correlation function between the received and reference functions. The second term is due to the noise falling within the data-rate bandwidth, and the final term is that due to the fraction of the frequency-spread CW interference falling within the data-rate bandwidth.

Assuming that $f_{ref}(t)$ is at base band, i.e. having a spectrum extending from zero Hertz, and that it has a frequency notch which encompasses the frequency of the interferer, the result of $f_{ref}(t) \cdot j(t)$ will have a frequency notch centred around 0 Hz. Figure 4 shows the spectrum of a binary sequence of 128 chips with a notch of ±8 bins, and a CW interferer overlaid at the notch centre frequency. The signal to interference power ratio is approximately -1.0 dB.

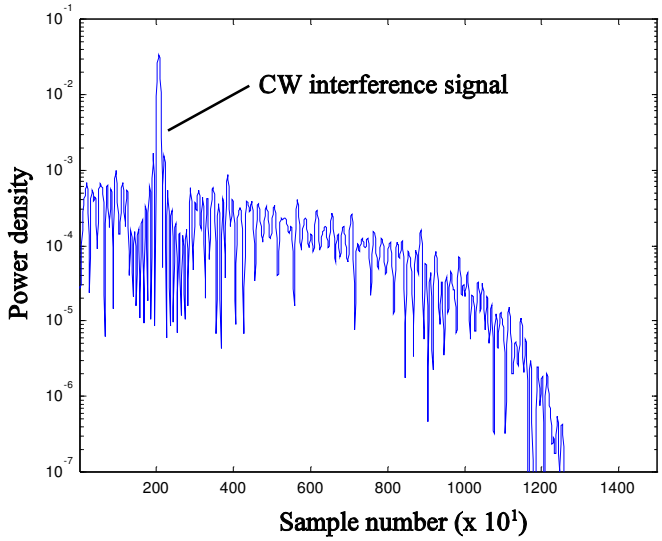

Figure 4 Frequency spectrum of binary spreading function at baseband with CW interferer. *Rectangular window.* SJR = -1.0 dB, SNR = +∞ dB.

The result of *multiplying* the notched binary sequence, $f_{ref}(t)$, and the CW interferer, $j(t)$, will produce the spectrum shown in figure 5. Spectral leakage, caused by rectangular windowing, may be clearly seen around the interferer in figure 4 and within the data-rate bandwidth in figure 5.

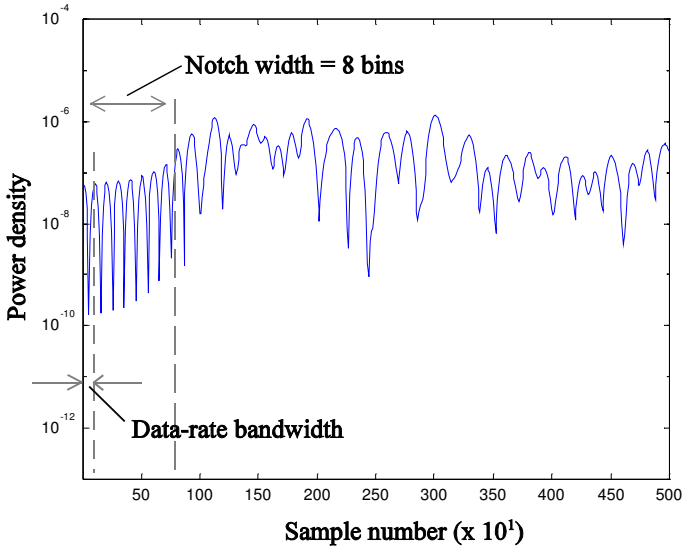

Figure 5 Significant spectral leakage occurs with a rectangular window function.

A tapered window function will significantly reduce the spectral leakage. Figures 6 and 7 represent the same conditions as figures 4 and 5, but a Hanning window has been applied to the time domain binary sequence.

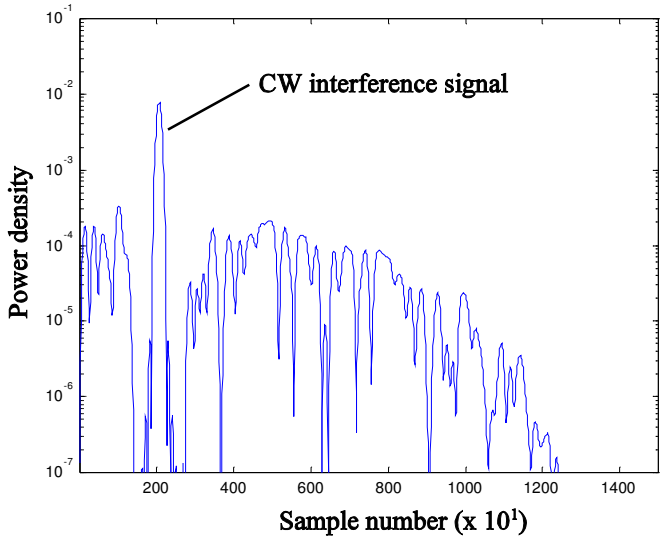

Figure 6 Frequency spectrum of binary spreading function at baseband with CW interferer. *Hanning window.* SJR = -1.0 dB, SNR = +∞ dB.

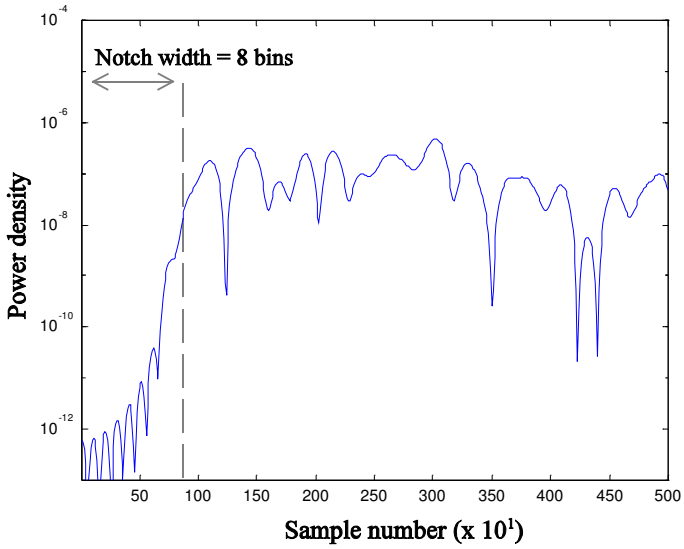

Figure 7 Spectral leakage is reduced with a tapered window function.

The window function may be positioned at the receiver input but it is more convenient to window the locally generated reference function (figure 8).

a) Window function at receiver input.

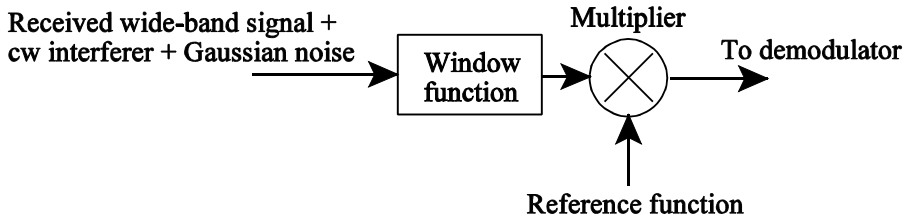

b) Windowing the reference function.

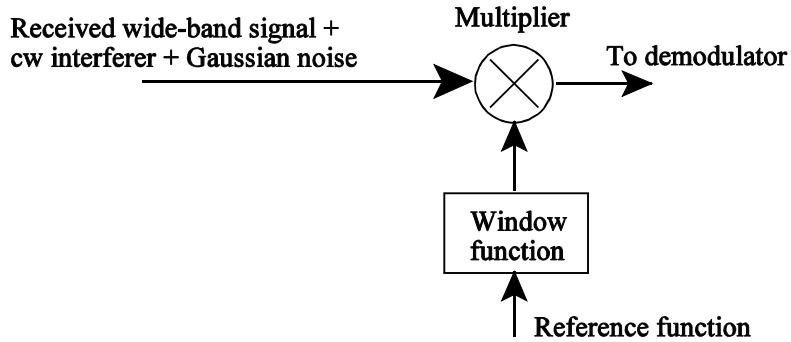

Figure 8 Applying a window function to the received signal.

2.2.1 Null width as a function of SJR.

The fixed frequency unmodulated interferer is truncated to the Fourier transform block length, hence a frequency null of width ±1 bin should entirely excise the energy from the main lobe of the interferer at the multiplier output. However the energy in the spectral sidelobes alone would be sufficient to compromise the demodulated bit error probability. The null width need only be sufficient to encompass the main frequency components of the truncated interferer (figure 9); further increases in null width would only marginally reduce the effect of the narrow band interferer but would further degrade the receiver performance in the presence of wide band Gaussian noise. The optimum null width is therefore a compromise between effective jammer excision and loss of process gain to AWGN, and will be dependent upon the signal to jammer power ratio at the receiver input.

Figure 10, which was a result of simulation using a random phase function with a rectangular window, a received signal to noise ratio of +7.0 dB, and a swept frequency interferer, illustrates how the receiver output bit error probability changes with null width and signal to jammer power ratio. From these tests the optimum null width for the range of SJR's used may be approximated by the straight-line relationship:

$$w_{opt} = 5.0 - [1.37 \times SJR(\text{dB})]\text{bins}$$

The corresponding graphs for the other three window functions are given in appendix 1. The results for the binary spreading function were obtained in the same manner, and are very similar. Table 1 gives the relationships used to calculate optimum null width versus SJR for all of the subsequent simulation tests taken, figure 11 illustrates the parameter w_{opt}.

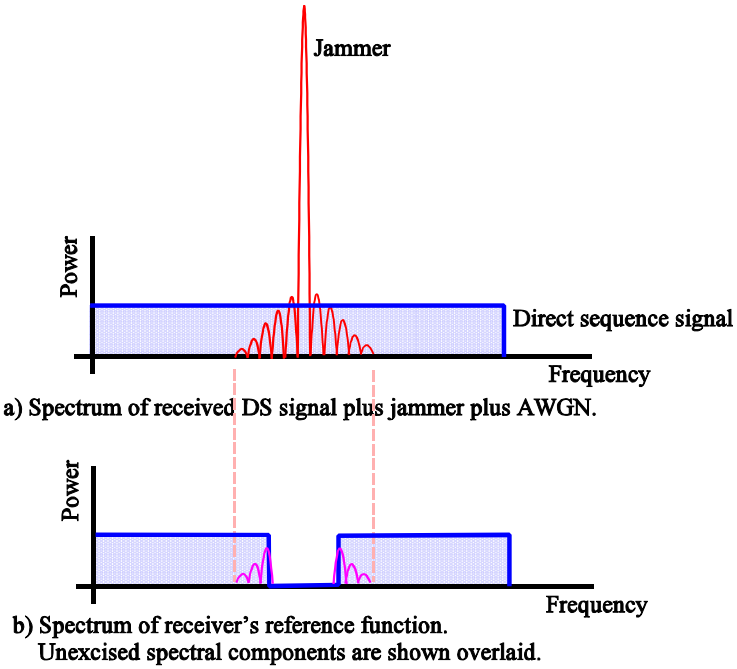

Figure 9 A high-power jammer will have significant spectral sidelobes.

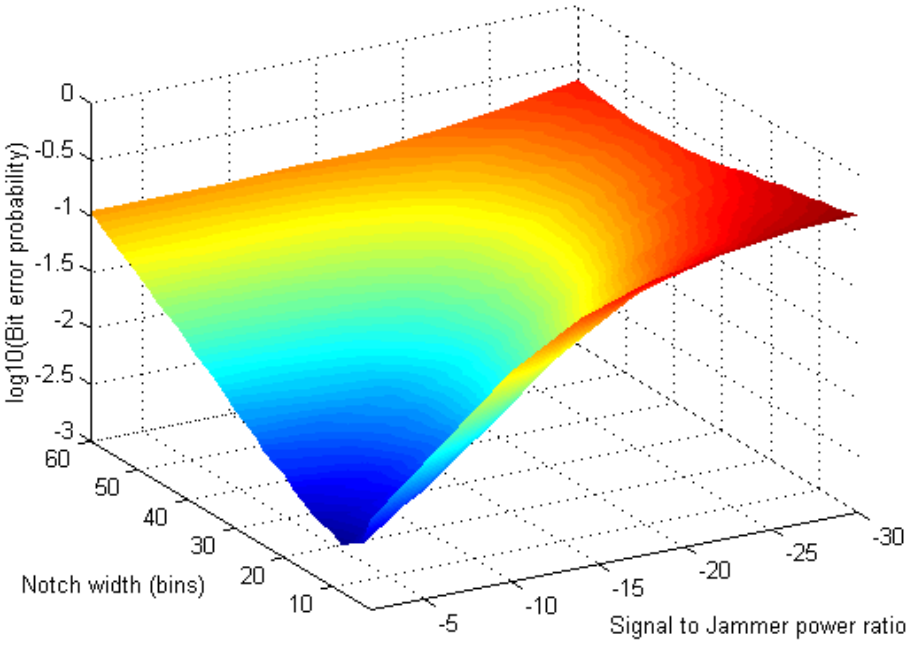

Figure 10 Determination of optimum null width as a function of SJR. Random phase function with rectangular window, SNR = +7.0 dB.

Window.	Binary pseudo-random function.	Random phase function.
Rectangular.	$w_{opt} = 7.7 - [0.91 \times SJR(\text{dB})]$	$w_{opt} = 5 - [1.37 \times SJR(\text{dB})]$
Hanning.	$w_{opt} = -[27.45 + 0.77 \times SJR(\text{dB})]$	$w_{opt} = -[33.3 + 0.89 \times SJR(\text{dB})]$
Blackman.	$w_{opt} = -[36.85 + 0.83 \times SJR(\text{dB})]$	$w_{opt} = -[40.84 + 0.91 \times SJR(\text{dB})]$
Blackman-Harris.	$w_{opt} = -[10.16 + 0.29 \times SJR(\text{dB})]$	$w_{opt} = -[10.55 + 0.31 \times SJR(\text{dB})]$

Table 1: Relationship between signal to jammer power ratio (SJR) and optimum null width w_{opt} (bins).

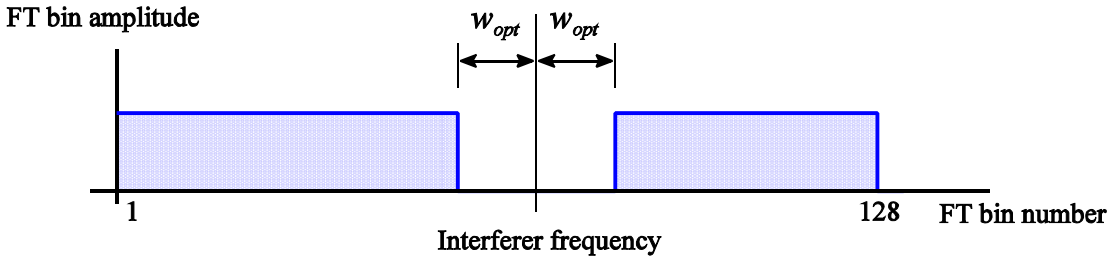

Figure 11 Showing the parameter w_{opt} in the spectrum of the random phase function.

2.2.2 Null width as a function of interferer frequency.

The binary pseudo-noise function will have a spectral envelope approximating to a $\text{sinc}^2(.)$ shape over one sequence period. Because of the shape of the envelope, spectral nulls located at the extremes of the main lobe will have less effect upon the process gain than those located toward the peak.

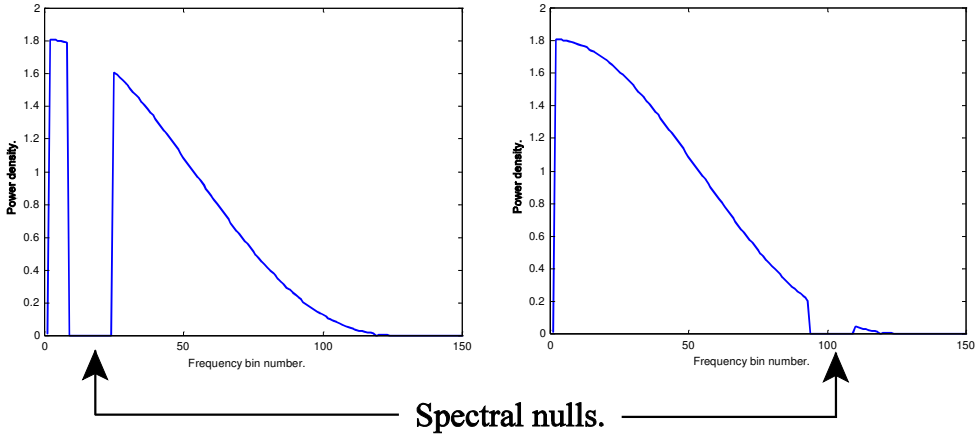

Figure 12 Spectral distribution of binary PRBS function, with nulls at extreme locations.

The random phase function has a flat spectrum, hence the reduction in process gain caused by

the nulled bins will remain constant irrespective of the null centre frequency within the signal main lobe.

Simulations to determine the effect of null width upon the recovered bit error probability for interferer frequencies across the spectrum of the binary spreading function produced results typified by figure 13, measured using a Hanning window. As expected, the bit error probability decreases for interferer frequencies toward the upper end of the spectrum.

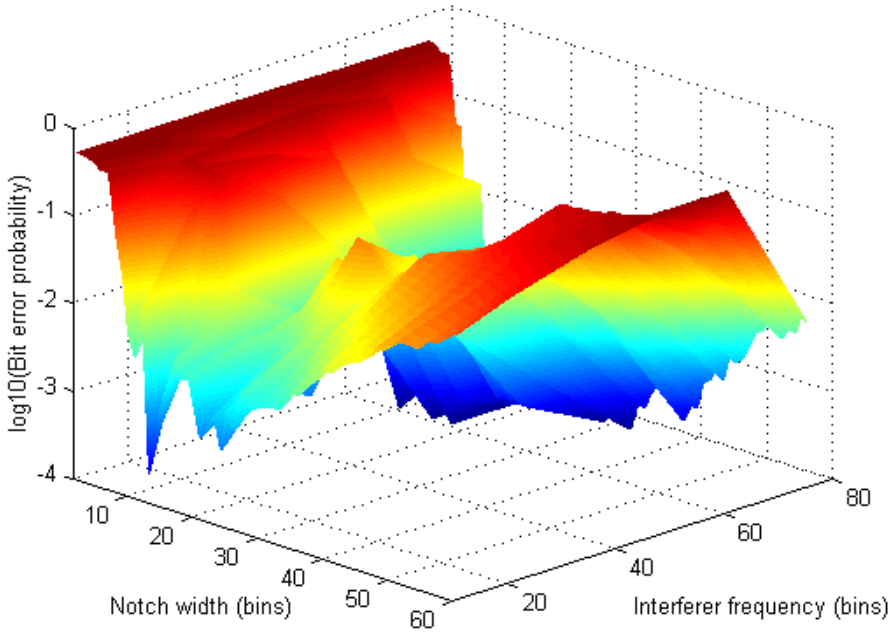

Figure 13 Null width versus interference frequency. Hanning window, binary PRBS function. E_b/N_o = +12 dB, E_b/N_J = -64 dB.

Figure 14 shows the same tests, also with a Hanning window, for the random phase function. It may be seen that the recovered bit error probability remains reasonably constant irrespective of the frequency of the interferer.

The main purpose of figures 13 and 14 is to illustrate that the optimum notch width for minimised bit error probability *does not* depend upon the interferer frequency, however for the binary spreading function the minimised bit error probability that is achieved *does* depend upon the interferer frequency. In order to average the frequency dependency of the binary sequence, the excision measurements presented in section 4 used a frequency swept interferer for both the binary and random phase functions. The frequency sweep range was between bins 22 to 102 for the simulation, and equivalently between 2.2 kHz and 10.0 kHz for the baseband hardware measurements.

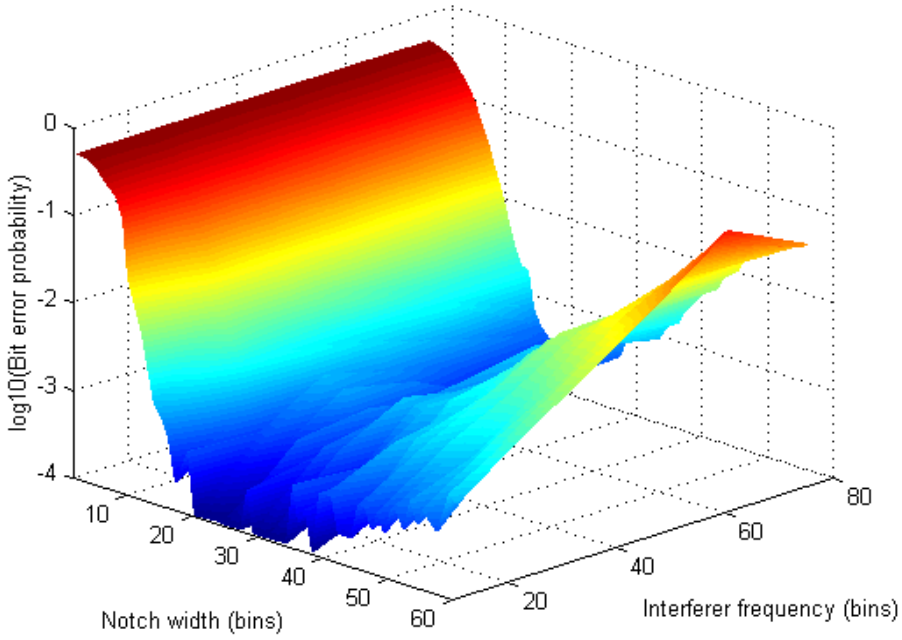

Figure 14 Null width versus interference frequency. Hanning window, random phase function. E_b/N_o = +12 dB, E_b/N_J = -64 dB.

2.3 Data bit error probability against added white Gaussian noise (AWGN).

The process gain for the baseband system is equal to $\frac{R_c}{R_b} = \frac{\text{chip rate}}{\text{bit rate}}$ for the binary spreading function, and equivalently the number of non-zero spectral lines in the Fourier transform block for the random phase spreading function. In both cases the process gain (G_p) is 128. If the receiver's reference function is windowed by anything other than a rectangular window the recovered signal power, and hence the process gain against white noise, will reduce. Simulation results (figure 15) show the effect of different window functions on the relationship between bit error probability and signal to noise power ratio. This figure applies identically to the binary function and the random phase function.

The rectangular window should be used when there is no narrow-band interferer, as the signal to noise ratio at the demodulator output is maximised. The Hanning, Blackman and Blackman-Harris windows have respectively a poorer performance against white noise, with a reduction in the process gain exceeding 3 dB for the Blackman-Harris window. However, the sacrifice of process gain is heavily offset by a much improved bit error probability against narrow-band interference. A practical system should therefore select an appropriate window for the interference conditions present in the channel from instant to instant.

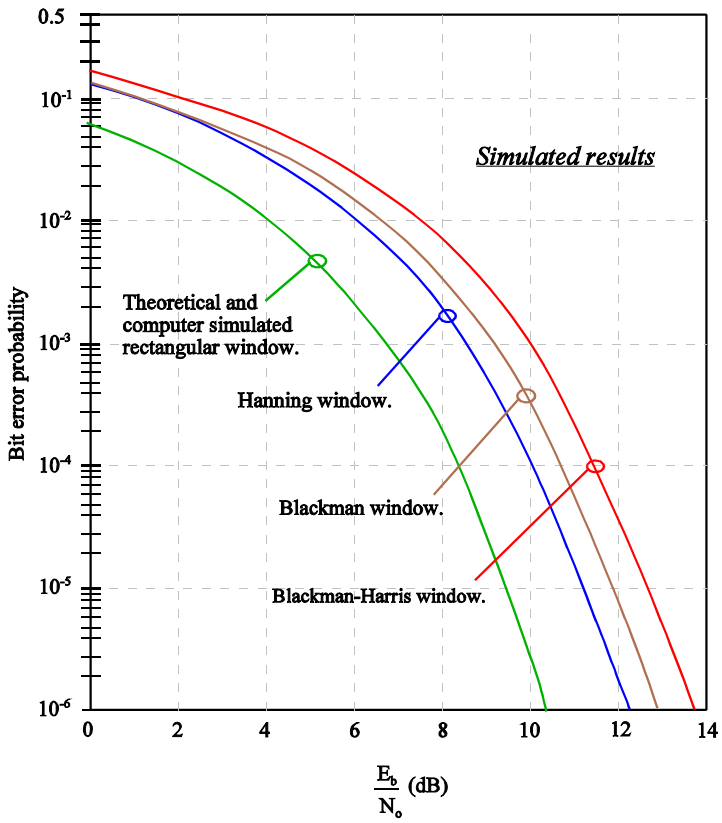

Figure 15 Comparison of bit error probability versus SNR for AWGN interference. Binary and random phase functions.

2.4 Excision of single CW jammer.

A single, unmodulated jamming tone was applied to the receiver input in order to determine the excision achievable by reference code nulls. The tone was generated as time domain samples with a frequency chosen such that there was a non-integer number of cycles within each Fourier transform block, this ensured that aliasing spectral sidelobes were present, as would be expected for a practical realisation. The frequency was linearly swept, as discussed in section 2.2.2, by stepping the frequency at the start of each block. The start phase of each block was randomly selected between 0 and 2π radians. The sweep rate was limited to ensure that the receiver could adapt its reference function to follow the frequency changes; a new adaptation frequency mask was calculated for each sequence (each data bit). A fixed level of white noise was also included to give a signal to noise power ratio, $\frac{E_b}{N_o}$, of +12 dB. Figure 16 plots bit error probability against $\frac{E_b}{N_J}$ for the random phase spreading function with a *rectangular* window, where E_b is the energy per bit and N_J is the interference power density,

$$N_J = \frac{J}{B_{ss}} = \frac{\text{Jammer power (watts)}}{\text{Signal main lobe bandwidth (Hz)}}.$$

The excision null width was optimised for the received signal to jammer power ratio, as discussed in section 2.2.1. The excision achieved at a bit error probability of 10^{-2} is 22 dB.

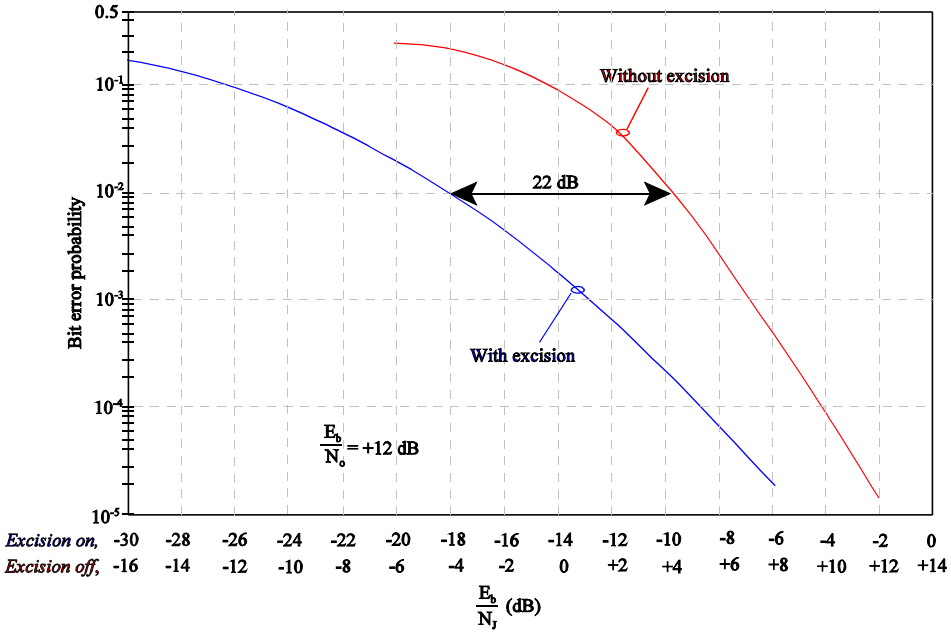

Figure 16 Jammer excision, random phase function with rectangular window.

Figures 17 and 18 show the best results achieved by the simulation for the random phase and binary spreading functions using the Blackman-Harris window, providing an excision of 103 dB and 105 dB respectively at a bit error probability of 10^{-2} against the CW interferer. The full set of graphs is presented in appendix 1.

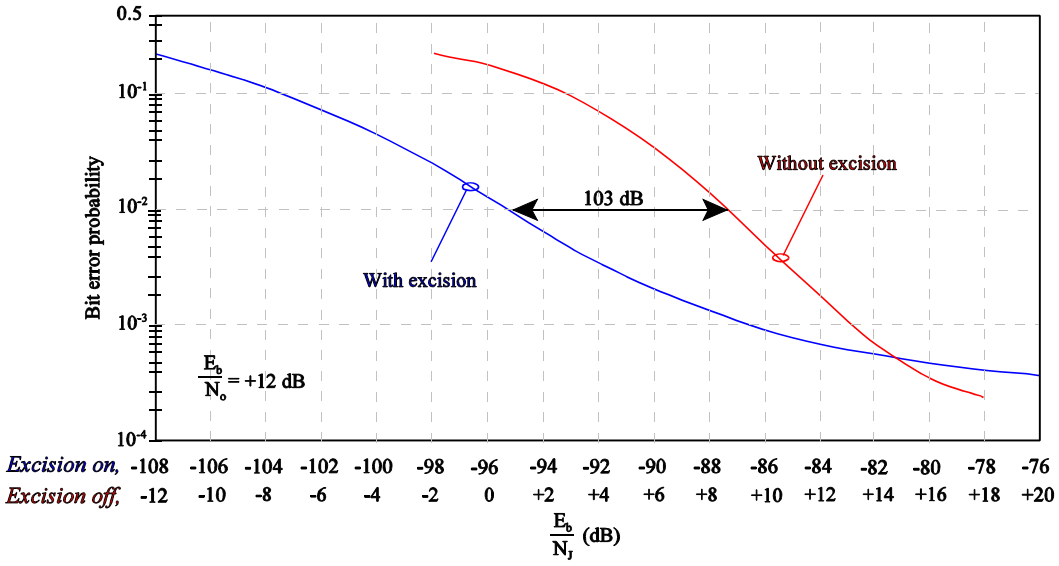

Figure 17 Jammer excision, random phase function with Blackman-Harris window.

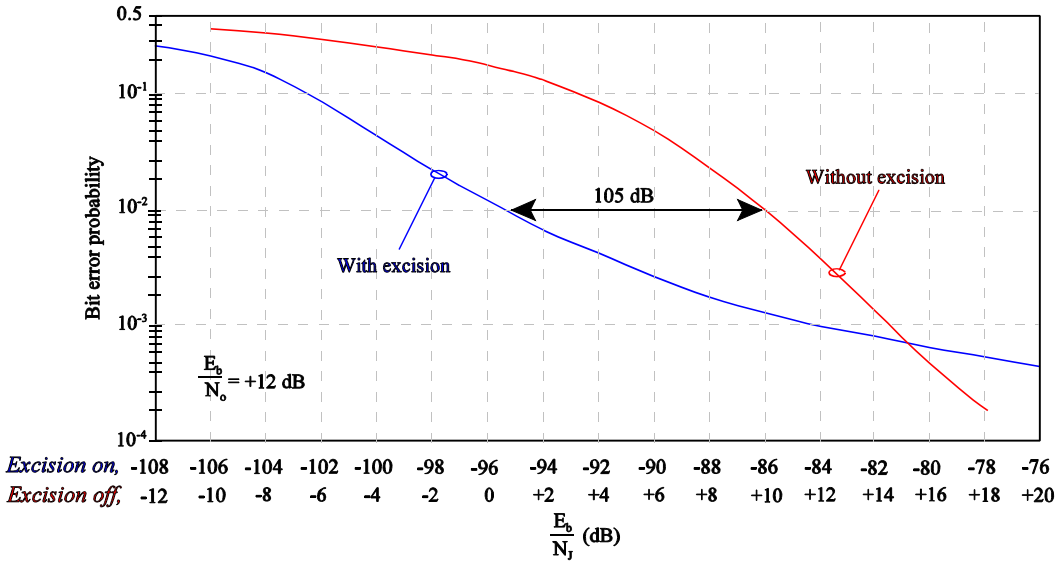

Figure 18 Jammer excision, binary pseudo-random function with Blackman-Harris window.

Tables 2 and 3 present excision results from the simulations for the baseband system employing a random phase spreading function and a binary pseudo-random spreading function respectively.

Window function	G_p reduction (window alone)	Jammer excision at BEP = 10^{-2}	SNR (E_b/N_J) at BEP = 10^{-2}
Rectangular	0.0 dB	22.0 dB	-18.0 dB
Hanning	2.0 dB	83.0 dB	-77.0 dB
Blackman	2.6 dB	90.0 dB	-83.0 dB
Blackman-Harris	3.2 dB	103.0 dB	-95.0 dB

Table 2: Summarised results for random phase function.

Window function	G_p reduction (window alone)	Jammer excision at BEP = 10^{-2}	SJR (E_b/N_J) at BEP = 10^{-2}
Rectangular	0.0 dB	17.0 dB	-11.2 dB
Hanning	2.0 dB	74.0 dB	-66.0 dB
Blackman	2.4 dB	81.0 dB	-72.2 dB
Blackman-Harris	3.1 dB	105.0 dB	-95.2 dB

Table 3: Summarised results for binary PRBS function.

2.5 Discussion.

Simulations have shown that excision of narrow-band interferers from direct sequence spread spectrum receivers may be successfully accomplished by removing (nulling) appropriate spectral bins from the reference function. In order to achieve maximum excision when the interfering signals at the receiver input consist of both Gaussian noise and narrow-band interference, the null width must be a function of the received signal to jammer power ratio. Shaping the reference function by time-domain windowing is essential to reduce spectral leakage caused by truncation of the Fourier transform block.

The simulations have compared the excision achievable using two different spreading / despreading functions, a binary sequence of 64 chips and a spectrally flat random-phase function with equivalent process gain. The degree of excision obtainable with the random phase function is largely unaffected by the frequency of the CW interferer in relation to the direct sequence carrier frequency. A short m-sequence (i.e. one that repeats its code for each data bit / FFT block) has a characteristic $\text{sinc}^2(.)$ power spectrum. Frequency bins that are removed close to the carrier represent a greater loss of signal power, and hence a loss of process gain, than those removed at frequencies close to the edge of the main lobe. When the sequence length of the binary code is greater than the bit duration, each Fourier transform block will contain a code that is not an m-sequence, and which could have undesirable spectral peaks (figure 19).

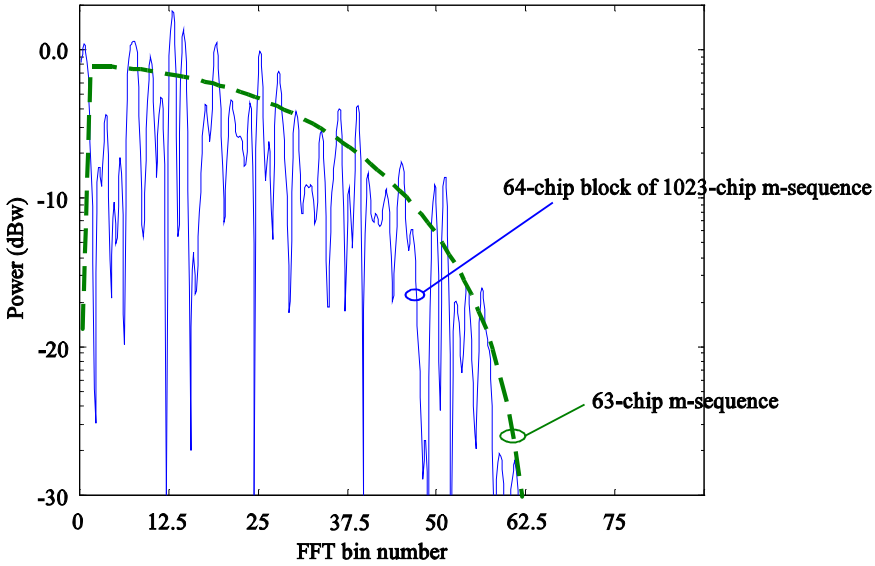

Figure 19 Comparison of power spectrum envelope of 64 chip block selected from m-sequence of length 1023 chips, and 63-chip m-sequence.

These spectral peaks represent vulnerable frequencies to non-excised cw interferers, or if spectral null excision is used their removal can represent a considerable loss of process gain to white noise.

The power spectrum of the random phase function contains no peaks, and hence will be less vulnerable to narrow-band interference.

The simulation results show that, except for the Blackman-Harris window, the random phase function with excision is more robust to swept-frequency narrow-band interference than a binary sequence with equivalent process gain. For the Blackman-Harris window the excision results are practically identical.

The excision levels of up to 105 dB., obtained by simulation, are unlikely to be achieved in practice because of limitations due to dynamic range and crosstalk from very high interferer power levels. This is discussed in chapters 3 and 4.

Chapter 3

3.1 Hardware demonstrator of baseband adaptive system with reference code windowing.

The first report describes the baseband hardware demonstrator based upon AT&T DSP32C digital signal processing cards in an IBM personal computer host platform, and associated software. Modifications to the 'receiver' software allowed the application of time domain windowing to the reference function. The window functions selected were those used for the simulations described in chapter 2, i.e.:

Rectangular (no windowing),
Hanning,
Blackman,
4-term Blackman-Harris.

Figure 20 shows a layout of the demonstrator.

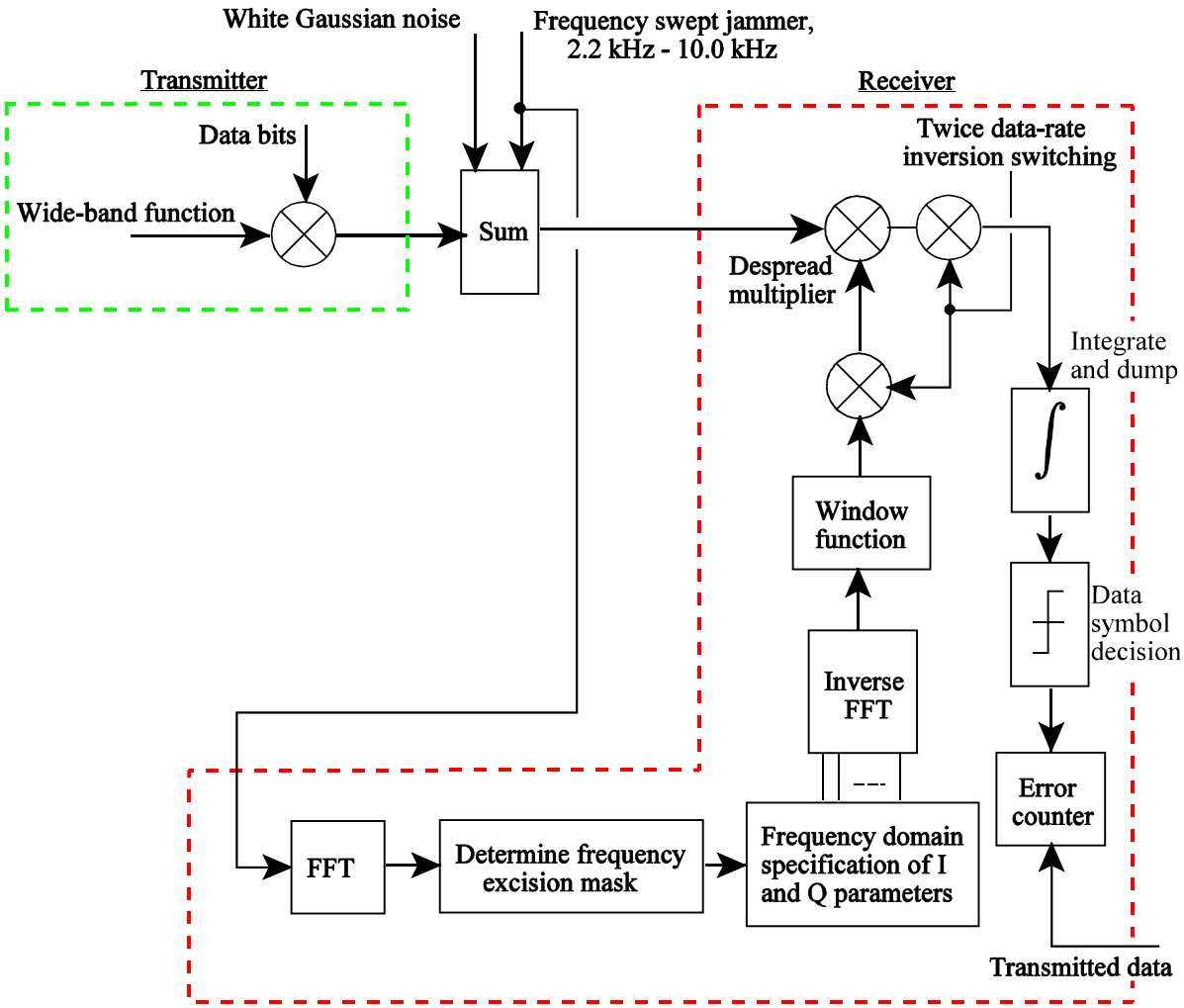

Figure 20 Test bed demonstrator used for excision measurements.

3.2 Process gain reduction due to reference function windowing.

Figure 21, obtained by measured results on the baseband system with a pseudo-random binary spreading function, shows how the bit error probability versus signal to noise ratio is degraded by reference code windowing. The basic performance of the system with a rectangular window is approximately 2 dB worse than the theoretical results for a binary PSK system:

$$P_b = \frac{1}{2} erfc \sqrt{\frac{E_b}{N_o}}$$

With respect to the rectangular window, the process gain reduction for the Hanning, Blackman and Blackman-Harris windows compares closely with the simulated results presented on page 12, figure 15.

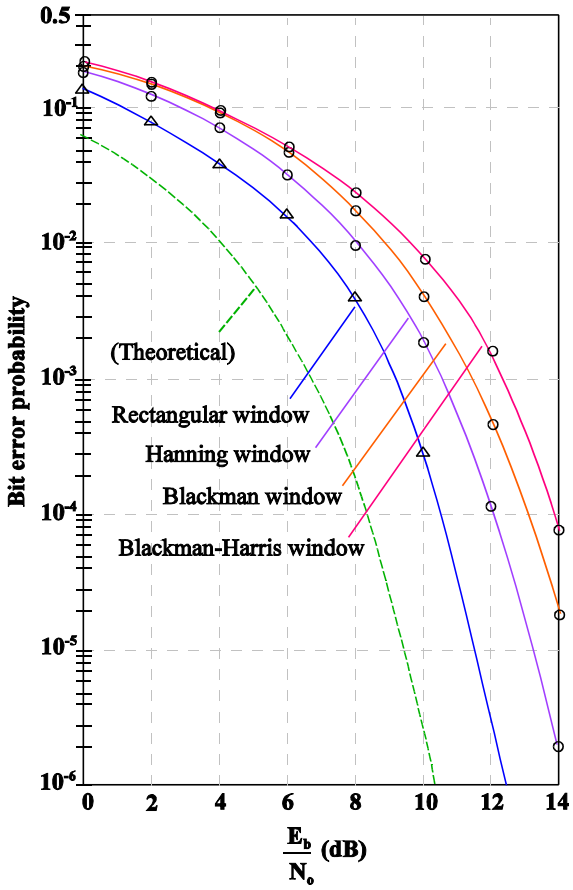

Figure 21 Performance degradation against white noise
for Pseudo-random binary spreading function (baseband system).

Figure 22 shows an identical set of measurements for the random phase spreading function. Compared to the binary spreading function, figure 22 indicates that the process gain with a rectangular window is poorer by approximately 1 dB, whilst the process gain for the other three window functions is improved by approximately 1 dB. The simulation measurements on page 12 show identical performance for the binary and random phase functions; therefore no significant conclusion may be drawn from the differences measured on the hardware demonstrator. Practical experience with the equipment showed that the performance was affected by the signal levels applied to the receiver's despread modulator. Whilst consistent

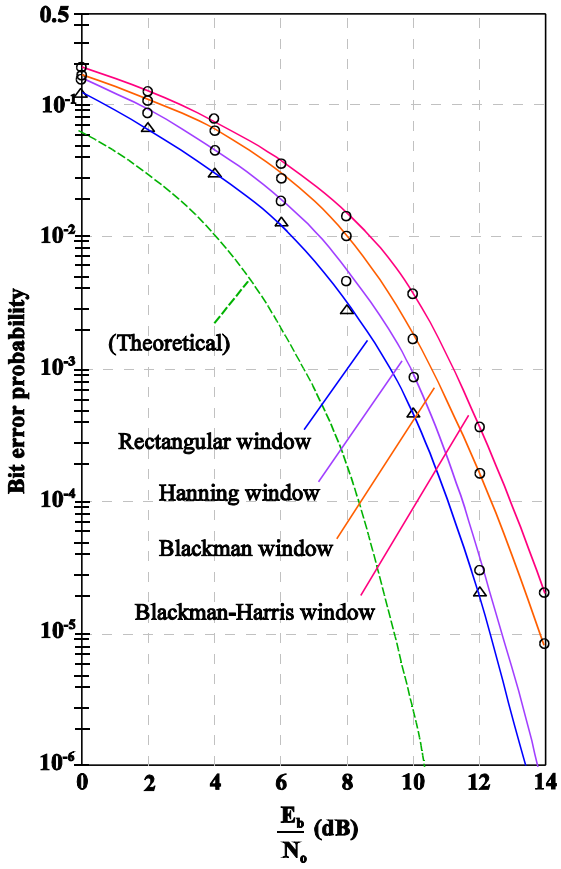

Figure 22 Performance degradation against white noise for random phase spreading function (baseband system).

peak drive voltages were maintained between the two different spreading functions, the wide dynamic range of the random phase function meant that there was a considerable difference in variance between the random phase and the binary reference signals. The problem of wide dynamic range for the random phase function, coupled with the limitations on peak signal voltage excursions inherent with the practical circuit implementation, later proved a major drawback when carrying out tests with carrier modulation.

3.3 Excision of narrow-band interference.

Section 2.2.1 (page 7) discusses optimum null width as a function of SJR, determined by computer simulation. The hardware measurements presented in this section and in chapter 4 were, however, taken before the simulation tests. The null width used for these measurements was chosen to agree with the initial work which culminated in the first report. In retrospect, it is considered that the level of jammer excision presented in this section and in chapter 4 could be increased by a further 6 to 8 dB had the null width been optimised. Unfortunately, time constraints have prevented further hardware tests prior to the compilation of this report.

Excision tests were made with a constant signal to noise ratio E_b/N_o of +12 dB, where the noise was spectrally flat Gaussian distributed. The CW interferer was linearly swept in frequency between 2.2 kHz and 10.0 kHz. Excision results for the rectangular window have

been presented in the first report, giving 8 dB interference rejection for the binary spreading function and 15 dB rejection for the random phase spreading function.

Windowing should improve the level of CW interference rejection at the expense of a reduction in process gain to white noise. Figure 23 presents a set of measurements for bit error probability against signal to jammer power ratio for the random phase function across all four windows. Figure 24 presents an identical set of tests for the binary pseudo-random function.

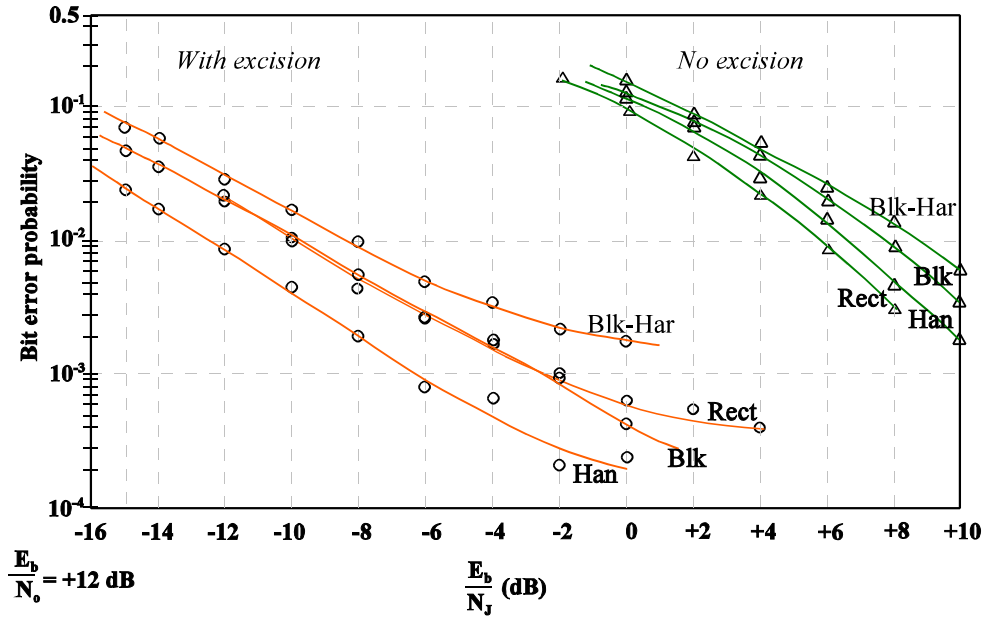

Figure 23 Random phase function, baseband system.

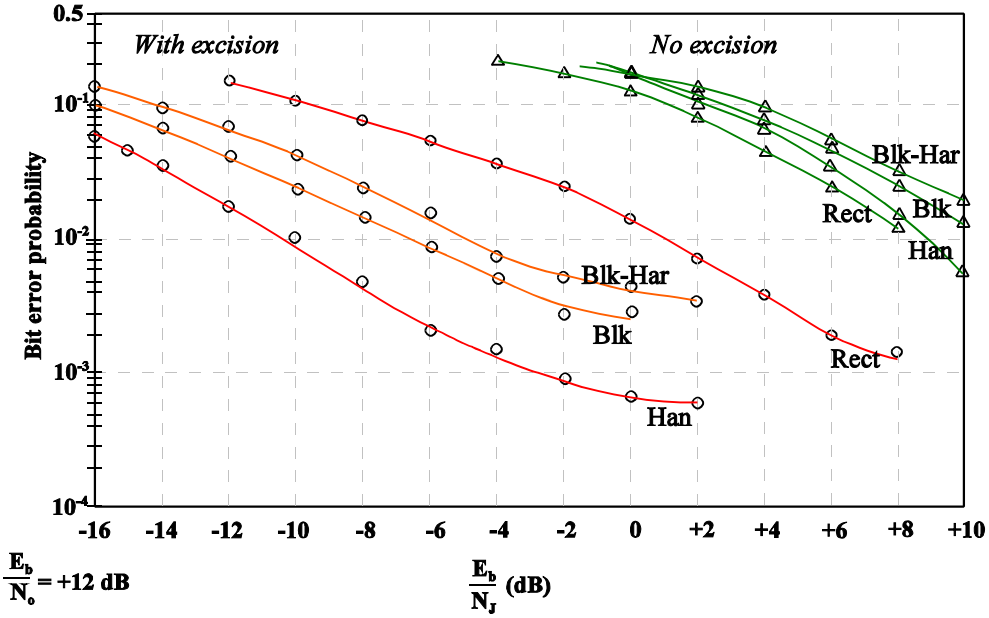

Figure 24 Binary pseudo-random function, baseband system.

Tables 4 and 5 present summarised results for the random phase and binary spreading functions respectively.

Window function	G_p reduction with respect to rectangular function	Jammer excision at error probability = 10^{-2}	E_b/N_J at error probability = 10^{-2} with excision
Rectangular	0.0 dB	15.0 dB	-9.7 dB
Hanning	0.5 dB	19.0 dB	-12.4 dB
Blackman	1.3 dB	17.3 dB	-9.7 dB
Blackman-Harris	1.8 dB	17.0 dB	-8.3 dB

Table 4: Summarised results for random phase spreading function (baseband system).

Window function	G_p reduction with respect to rectangular function	Jammer excision at error probability = 10^{-2}	E_b/N_J at error probability = 10^{-2} with excision
Rectangular	0.0 dB	7.0 dB	+1.0 dB
Hanning	1.2 dB	19.1 dB	-10.4 dB
Blackman	1.8 dB	17.0 dB	-6.5 dB
Blackman-Harris	2.7 dB	17.2 dB	-4.9 dB

Table 5: Summarised results for pseudo-random binary spreading function (baseband system).

Although the level of interference signal rejection for all except the rectangular window is similar between the two different spreading functions, the bit error probability for the excised and non-excised interferer is lower (i.e. improved) for the random phase function by approximately 2 dB signal to jammer power ratio.

From figures 21 and 22 it may be seen that with a signal to noise ratio of +12 dB, Blackman-Harris windowing and with no spectral null in the reference function, the bit error probability will have a floor of approximately 4×10^{-4} for the random phase function and 1.5×10^{-3} for the binary function. This floor will be slightly higher with the excision notch present due to the extra reduction in process gain of 0.58 dB (for a notch of ±8 bins).

The measured results presented in tables 4 and 5 are considerably less dramatic than those of tables 2 and 3 (page 14), which were achieved by simulation. Although simulation results for levels of rejection in excess of 100 dB could not be expected to be approached in practice, the actual maximum level achieved of 19.1 dB is clearly disappointing.

There are a number of problems that can arise in a practical implementation that do not exist in a computer simulation. For example, the dynamic range of a software simulation is limited only by the range of the floating point number representation, 3.4×10^{-38} to $3.4 \times 10^{+38}$. There

are no problems of crosstalk or signal breakthrough no matter how small the signal to jammer power ratio. All circuits can be perfectly linear, and therefore intermodulation distortion will not occur. These issues can only be addressed in a practical realisation by extremely careful design.

A carrier modulated system was trialed in order to investigate the extent to which crosstalk, between the input and output of the double-balanced modulator at the receiver, compromised the jammer excision. This is discussed in the following chapter.

Chapter 4

4.1 Hardware based adaptive system with carrier modulation.

A block diagram of the carrier modulated system is shown in figure 25. A relatively low carrier frequency of 80 kHz was selected for the following reasons:

a) Much of the existing equipment could be used without the extensive modifications that would be required in order to operate at higher frequencies.

b) The frequency was sufficiently high to ensure that cross talk or breakthrough from unwanted signal or interference components around the carrier frequency would lie well outside of the data bandwidth and would not effect the data decision circuits.

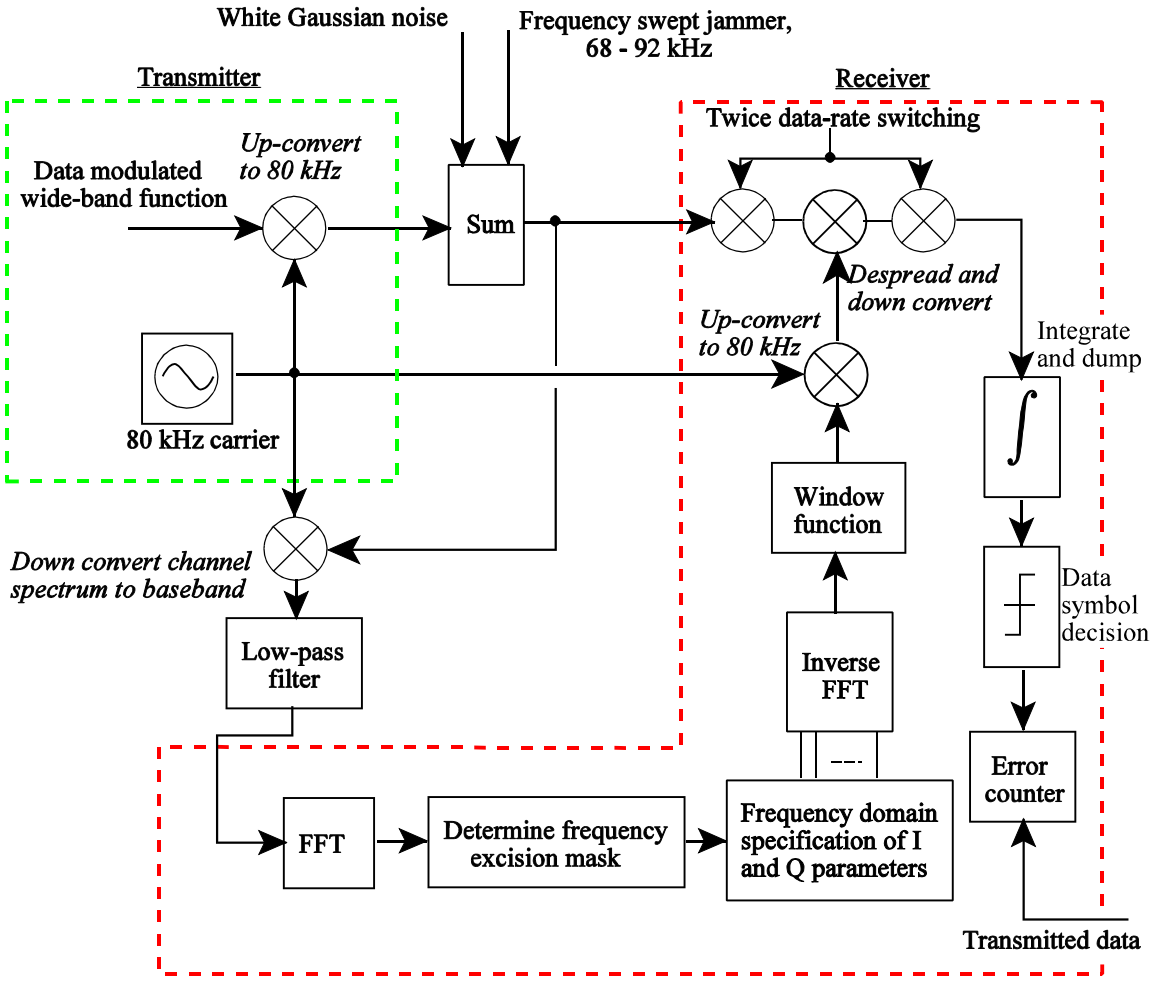

Figure 25 Test bed used for excision measurements on carrier modulated system.

The bandwidth of the modulated wide band signal extends from 67.5 kHz to 92.5 kHz. The interfering CW signal was swept in frequency across the spread bandwidth, however as it approached the carrier frequency (at 80 kHz) the down-converted representation at the receiver channel monitor input approached 0 Hz. This low frequency 'difference' signal was unsuitable for determining the frequency excision mask and the frequency notch would

momentarily disappear as the jamming signal swept across the carrier frequency. A CW interferer at (or close to) the carrier frequency is a worst-case situation for a direct sequence receiver for the following reasons:

a) The power density of the wide band binary function is maximum around the carrier frequency ($sinc^2(.)$ spectrum), hence the interference power within the data rate bandwidth is maximised.

b) Any residual carrier component on the wide band reference as a result of incomplete carrier suppression will combine with the CW jammer and place interference power directly into the data rate bandwidth.

These problems were addressed by careful adjustment of the receiver's carrier modulator to optimise carrier suppression, and by permanently setting bins 1 to 8 of the transmitted and reference functions to zero. However, the carrier suppression was still insufficient to prevent bursts of errors occurring whenever the jamming signal was within ±100 Hz of the carrier frequency.

For the baseband system, the reference function at the input to the receiver's de-spread multiplier was phase inverted at the mid-period of each data bit. The correct signal polarity was restored by further phase inversion switching of the signal at the multiplier output (see figure 20 on page 17). The purpose of this, as discussed in the first report, was to cancel any DC offset from the multiplier at the input to the integrate and dump filter. In order to preserve the shape and depth of the spectral null defined in the reference function the phase inversion switching was moved to the receiver input (see figure 25). However, computer simulation tests showed that neither of the inversion switching methods had any negative impact upon the level of jamming excision achieved.

The following other improvements were made to the hardware test bed, mainly to 'tidy-up' the system rather than to improve the excision performance:

- The receiver must determine the frequency of the interferer in order to set its frequency excision mask. Previously, the frequency was determined by comparing the absolute value of the magnitude for each Fourier transform bin with a fixed threshold, and assuming that any signal above the threshold was to be excised. This required an external level control to set the amplitude at the FFT input.

  The modified receiver software determined the average power level across all of the Fourier transform bins within the spread signal bandwidth, and compared the power level of each FT bin with this average value. A bin which exceeded the average by 20 times (13 dB) was assumed to represent a jamming interferer. Thus external signal level adjustments in response to SJR changes were no longer necessary.

- Changes to the excision null width or to the selection of a window function previously necessitated recompiling the DSP software. Modifications were made to allow these change to be carried out from the keyboard without the need for recompiling.

The relatively slow bit rate for the hardware system (97.7 bits/second) meant that error probability measurements were very time consuming. This is a further area where software simulation has advantages over a hardware implementation; many simulations, each with different parameters, may be run at the same time with the results saved to disc file for later collation. Even if an individual simulation takes several hours the computers may be left overnight or over a weekend without the need for intervention. A set of tests on the hardware system cannot be carried out in parallel as there was only one test bed available. As a result, measurements to determine the optimum excision notch width (as in chapter 2, sections 2.2.1 and 2.2.2) were not completed. This report presents results for the carrier modulated system that uses the same notch width as those in the tests on the baseband system. However, a limited set of measurements indicated that a further 6 to 8 dB improvement may be achieved with suitable optimisation of the notch width.

4.2 Frequency spectrum of wide-band function.

Figure 26 a) illustrates the spectrum of the 'transmitted' wide band signal; the receiver's reference function will be identical if there is no narrow band interference present. The enforced notch around the carrier frequency, as discussed in section 4.1 above, may be seen.

If an interfering signal is detected the reference function will be modified, as in figure 26 b). Because the frequency notch is formed prior to carrier modulation it will appear identically within both sidebands. For each window function, the excision notch width was identical to that used for the baseband measurements in section 3.3.

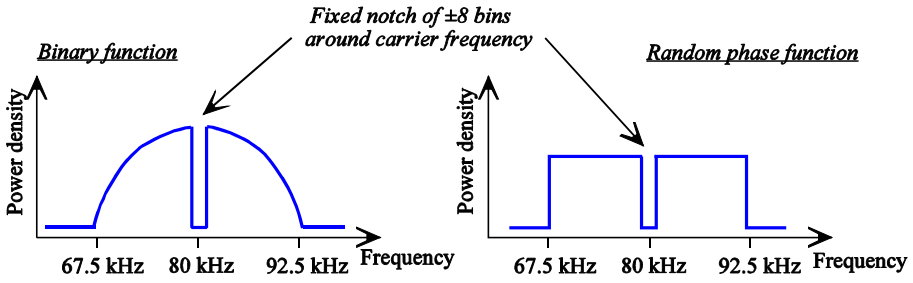

a) Transmitted spreading function.

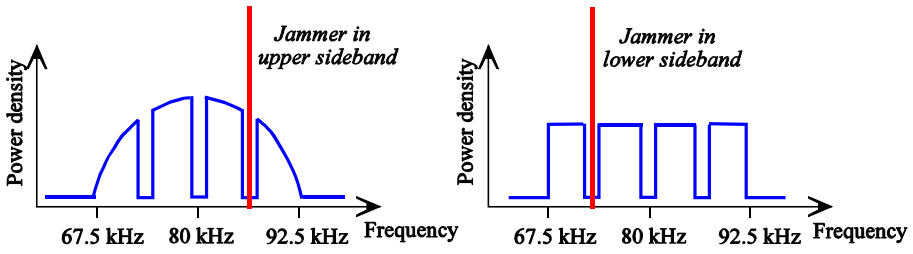

b) Reference despreading function.

Figure 26 Frequency spectra of wide-band function.

4.3. Data bit error probability against added white Gaussian noise.

The process gain for a modulated direct sequence system using a binary pseudo-random spreading function is given by:

$$G_p = \frac{\text{Spread bandwidth}}{\text{Bit rate}}$$

which is equivalent to:

G_p = 2 x number of chips per bit (binary sequence),

For the tests presented in this report the duration of the pseudo-random binary sequence is equal to the duration of each Fourier transform block, and each block represents one data bit. Hence the number of non-zero defined spectral bins in each FFT block is equal to the number of chips per bit, i.e. 128. The random phase function also has 128 non-zero defined spectral bins for each FFT block, and therefore the process gain for this function is:

G_p = 2 x number of non-zero frequency bins in main lobe bandwidth.

However, for both spreading functions, eight frequency bins to each side of the carrier are set to zero, hence the process gain for the binary and random phase functions is 2 x 120 = 240 (23.8 dB)

The signal to noise and signal to jammer power ratios were determined by individual measurements of the root mean square voltages for signal, noise and interference. Figure 27 shows the circuit layout. The method of generation for the binary and random phase functions ensures that the power of the modulated signal is tightly band limited to lie within the frequency range 67.5 kHz to 92.5 kHz. The added white Gaussian noise from the noise generator has no such constraint and extends both above and below the signal frequency.

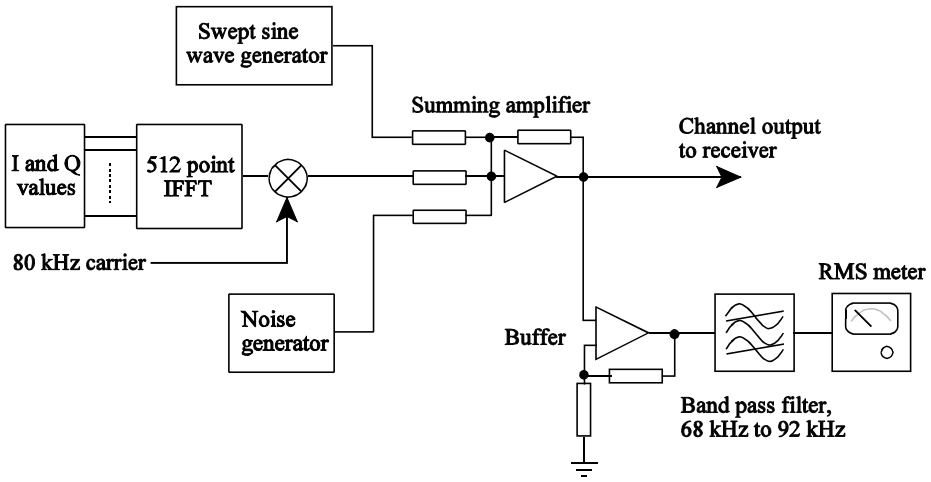

Figure 27 Showing method used for setting signal, noise and jammer power levels.

The band pass filter at the input to the root mean square voltmeter is present to ensure that both signal and noise powers are measured within the same bandwidth, however the filter roll-off characteristic means that the noise bandwidth at the voltmeter input is wider than the

3dB bandwidth of 68 kHz to 92 kHz. When setting the signal and noise voltages using calculations based upon an ideal filter characteristic, the actual noise power within the signal bandwidth will be less than the desired noise power and the results for bit error probability versus SNR would appear better than they should. (The measured results for the binary function were approximately 1 dB better than the theoretical prediction.) The graphs of figure 28, representing measured data bit error probability versus SNR for the carrier modulated system, have had their horizontal scale adjusted in order to match the curves for the rectangular window with those measured in the baseband tests in order to compensate for this effect.

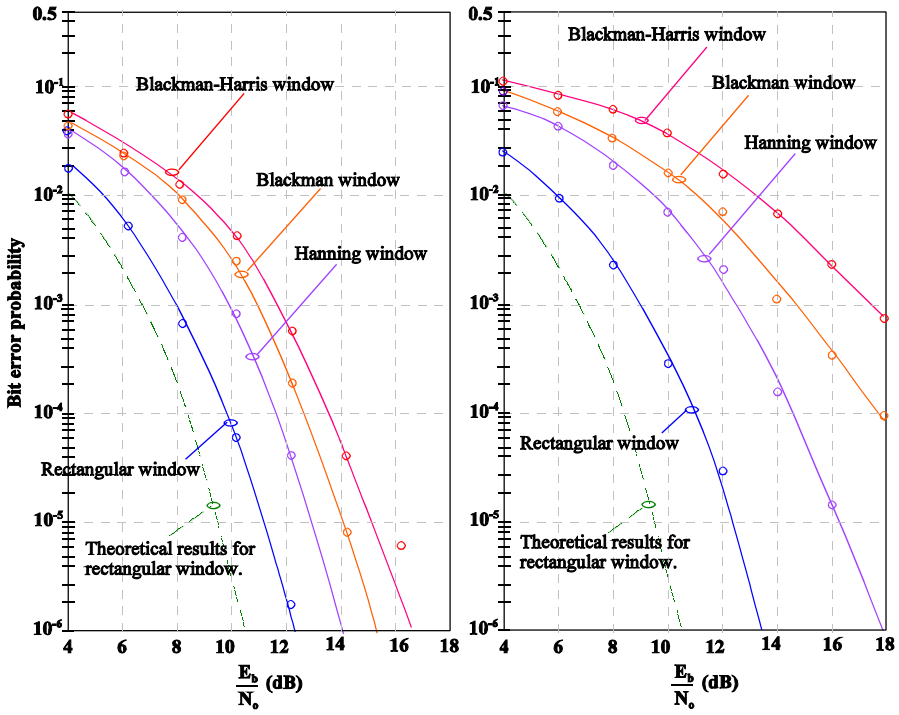

Figure 28 Comparison of bit error probability versus SNR for AWGN interference. Binary and random phase spreading functions.

Comparisons with the baseband results for the binary function (figure 21) show reasonably close agreement across all of the window functions. However, similar comparisons for the random phase spreading function (figure 22) returns a significantly poorer result for the carrier modulated system. The Blackman-Harris window has a process gain reduction in excess of 5 dB when compared with the baseband measurements.

The wide dynamic range of the random phase function, coupled with necessary limitations of the signal voltage excursions to avoid amplitude clipping, reduces the variance of the reference signal to the de-spread multiplier compared with that for the binary function. For the multiplier used, the signal to noise ratio at the output is compromised if the reference drive voltage at the input is too low. This problem was found to cause even greater degradation when investigating the excision performance discussed in the following section.

Experiments have shown that the demodulated signal to noise ratio for the random phase

function could be considerably improved if the reference function drive voltage at the multiplier input was increased to the point of severe clipping. However, the maintenance of a deep spectral null in the reference function, required for efficient narrow band interference excision, excludes any form of signal distortion, therefore signal linearity was preserved in all further tests.

4.4 The effect of jammer frequency upon the relationship between SJR and BEP.

The frequency-power spectrum of the pseudo-random binary function has a $\left(\frac{\sin x}{x}\right)^2$ relationship, whilst that of the random phase function has a constant power spectral density which extends across the main lobe bandwidth.

Figure 29 shows measured results for the pseudo-random binary function with a rectangular window, of bit error probability versus SJR for four different (fixed) jammer frequencies. Measurements were taken with excision 'on' and excision 'off', and with E_b/N_o = +12 dB. The carrier frequency is 80 kHz, and the lower and upper sidebands extend out to ±12.5 kHz from the carrier. The fixed frequency jammer is located at one of four frequencies within the lower sideband. The excision level remains approximately constant at 19 dB irrespective of the jammer frequency.

Figure 30 shows an identical set of measurements for the random phase function and rectangular window. As expected, the bit error probability versus SJR results are independent of jammer frequency.

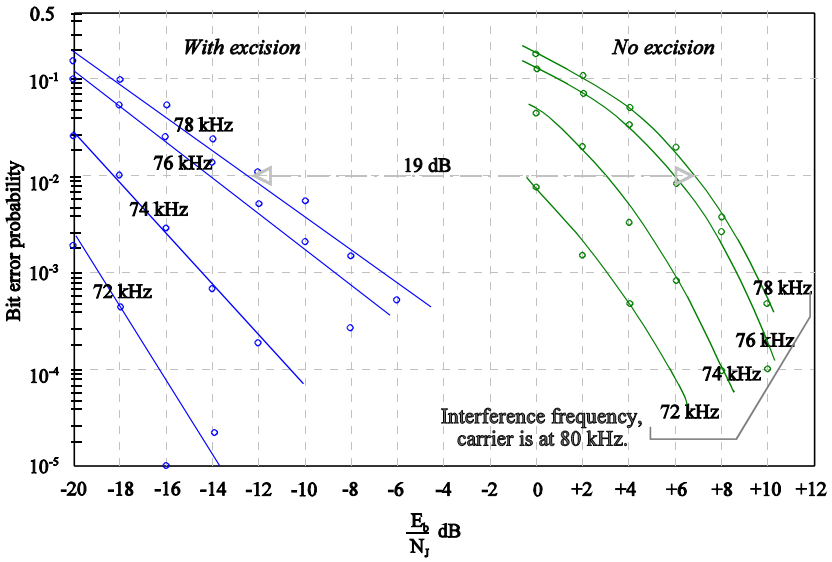

Figure 29 Binary function, rectangular window. Fixed frequency jammer. E_b/N_o = +12 dB.

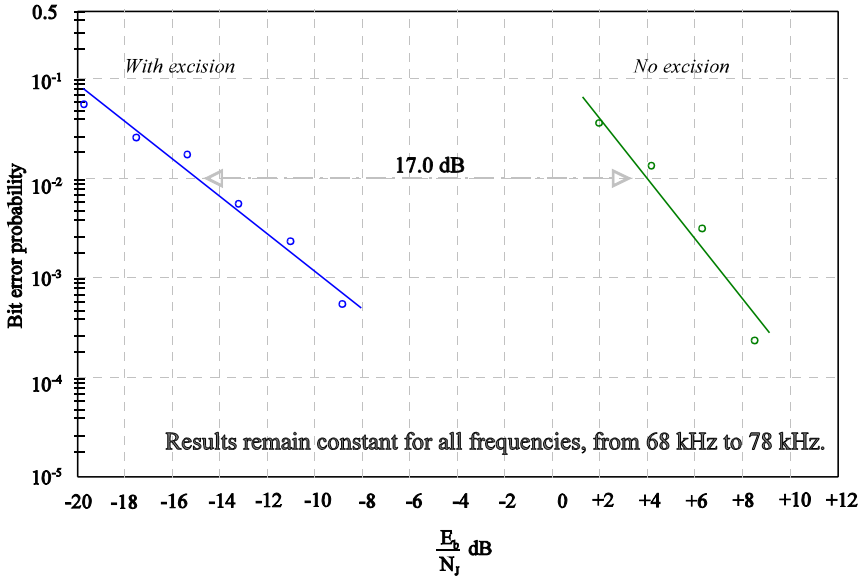

Figure 30 Random phase function, rectangular window. Fixed frequency jammer. E_b/N_o = +12 dB.

4.5 Excision of swept frequency single CW jammer.

The interfering sine wave was linearly swept across the main lobe bandwidth of the wide band signal, from 67.5 kHz to 92.5 kHz, including the sensitive area around the carrier frequency. Figure 31 shows the measured results for the binary wide band function, both with and without excision, for each of the four window functions with a fixed null width of ±8 bins.

Although the use of a tapered window function (i.e. Hanning, Blackman, etc) improves the level of excision achieved (i.e. the difference in SJR between the curves for excision 'on' and excision 'off'), the curves indicate that the absolute performance in terms of bit error probability for signal to jammer ratios (E_b/N_J) above -12 dB is highest for the rectangular window. This is somewhat at odds with results from both the simulation and the baseband measurements. Figure 31 also includes results from initial tests, made just prior to the compilation of this report, with larger excision null widths (±22 bins for the rectangular window, and ±18 bins for the Hanning window). These show a significant improvement in both the jammer suppression and the absolute performance, and indicate excision levels at BEP = 10^{-2} of approximately 16 dB for the rectangular window and 29 dB for the Hanning window.

Figure 32 shows the measured results for the random phase function, both with and without excision, for notch widths close to ±8 bins.

Comparisons between figures 31 and 32 show that results for the rectangular window are very similar, however for the other three windows the bit error probability versus SJR achieved by the random phase function is worse than that achieved by the binary pseudo-random function. This is due to the difference in mean signal levels between the binary and random phase functions as discussed at the end of section 4.3 (page 27).

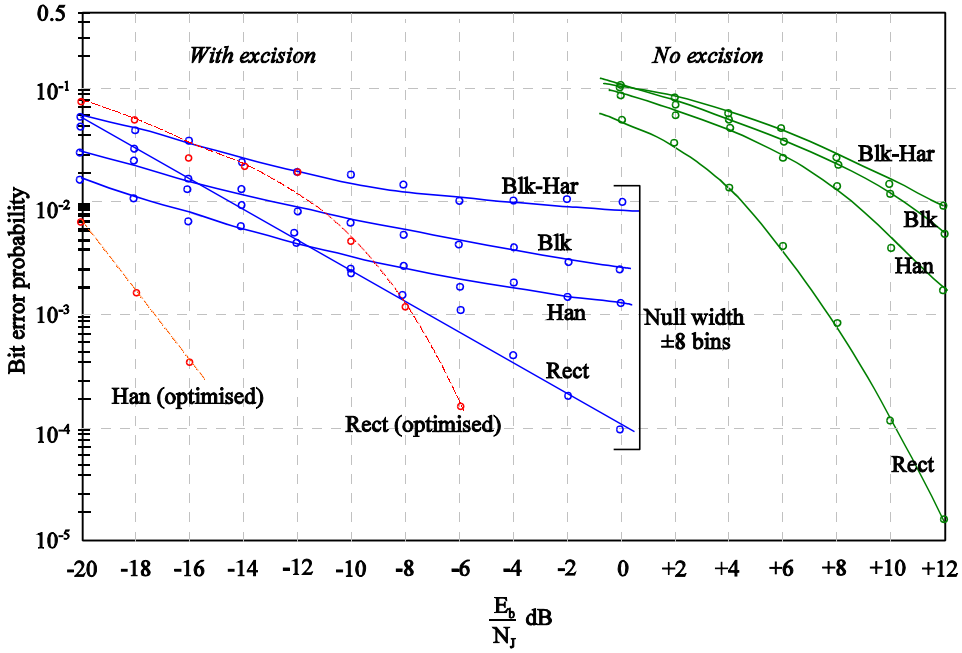

Figure 31 Binary pseudo-random function, carrier modulated.
Sweep frequency jammer. E_b/N_o = +12 dB.

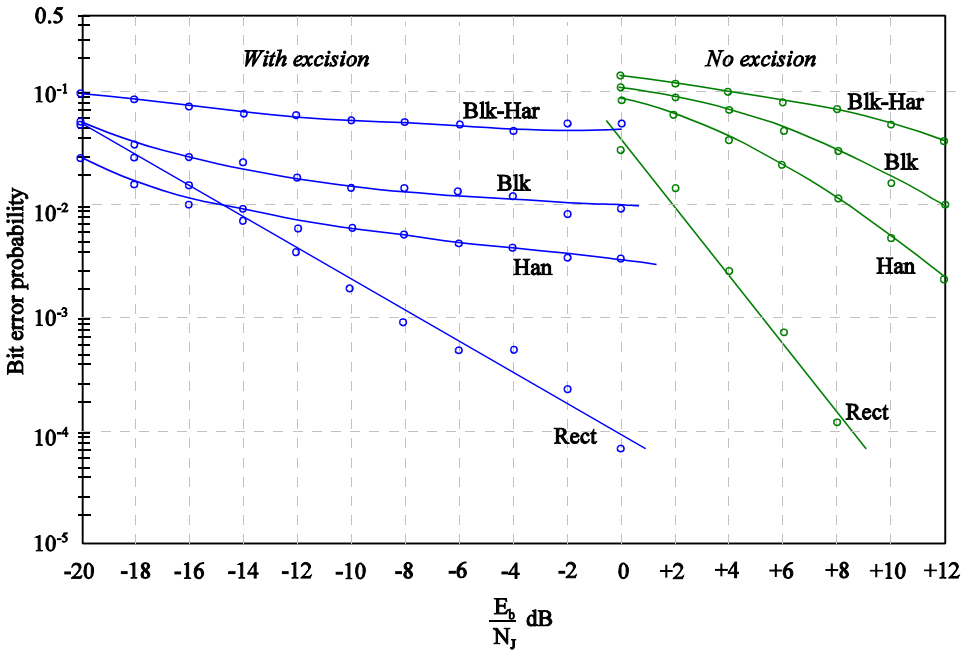

Figure 32 Random phase function, carrier modulated.
Sweep frequency jammer. E_b/N_o = +12 dB.

However, it is considered that with suitable optimisation of the signal levels and of the excision null width for each spreading function, the binary and random phase functions will have very similar performance in terms of available process gain and interference excision.

Tables 6 and 7 present summarised results for the random phase and binary spreading functions respectively, based upon the measurements presented in figures 31 and 32.

Window function	G_p reduction with respect to rectangular function	Jammer excision at error probability = 10^{-2}	E_b/N_J at error probability = 10^{-2} with excision
Rectangular	0.0 dB	16.8 dB	-15.0 dB
Hanning	3.5 dB	23.0 dB	-14.5 dB
Blackman	7.0 dB	12.0 dB	0.0 dB
Blackman-Harris	9.0 dB	-	-

Table 6: Summarised results for random phase spreading function (carrier system).

Window function	G_p reduction with respect to rectangular function	Jammer excision at error probability = 10^{-2}	E_b/N_J at error probability = 10^{-2} with excision
Rectangular	0.0 dB	18.5 dB	-14.5 dB
Hanning	2.0 dB	25.5 dB	-17.0 dB
Blackman	3.0 dB	23.0 dB	-12.5 dB
Blackman-Harris	4.0 dB	16.0 dB	-4.0 dB

Table 7: Summarised results for pseudo-random binary spreading function (carrier system).

The results for the random phase function with Blackman-Harris window have not been included, as a bit error probability of 10^{-2} could not be achieved with a signal to noise ratio of +12 dB.

4.6 Discussion.

Comparing the results for the binary spreading function, table 7 (carrier system) with table 5 (baseband system) the following observations may be made:

With a rectangular window function, the carrier modulated system shows an improvement of 11.5 dB in the level of excision, and will return a bit error probability of 10^{-2} for E_b/N_J = -14.5 dB as against +1.0 dB for the baseband system.

The Hanning and Blackman window functions also show an improvement in excision level, 6.4 dB and 6.0 dB respectively, and a lower SJR for error probability = 10^{-2} by 6.6 dB and 6.0 dB respectively. However the loss of process gain is slightly higher.

The Blackman-Harris window returns a slightly poorer result for the carrier modulated system across all of the measurements.

In order to achieve signal to jammer ratios down to -20 dB without having to apply a high

peak jammer voltage at the input to the despread multiplier (figure 33), the carrier modulated signal voltage was relatively low at 5 millivolts rms, and was kept at this level for all of the carrier modulated tests. To achieve a signal to jammer power ratio of -20 dB the jammer rms voltage was set at 800 millivolts.

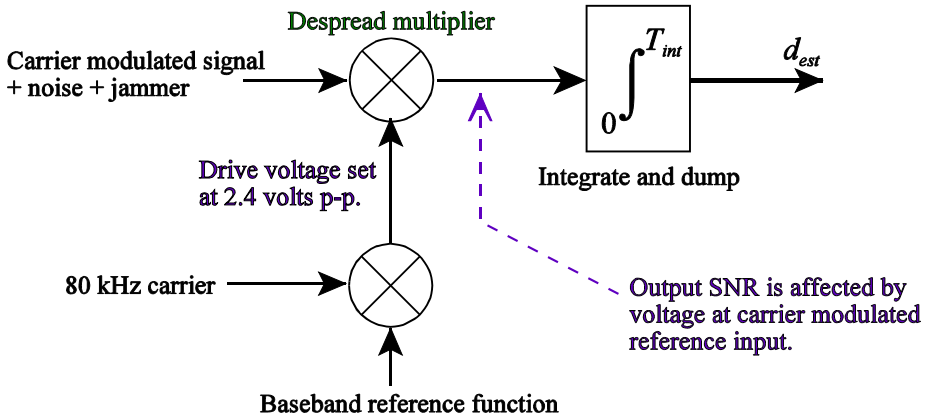

Figure 33 Despread correlator within the receiver.

With such a relatively low signal voltage it was found that the despread signal to noise ratio at the output of the receiver's multiplier was dependent upon the voltage level of the reference input. For all of the measurements on the carrier modulated system presented here, the reference input was set to a maximum of 2.4 volts peak to peak for both binary and random phase spreading functions; this level being dictated by limitations of the output voltage from the preceding frequency up-conversion multiplier. In retrospect this was found to be rather low, and was later increased to 8 volts peak to peak by including an amplifier between the two multipliers. Unfortunately, time limitations prevented retaking the excision measurements prior to the compilation of this report.

The tapered window functions, in particular the Blackman-Harris window, reduce the mean power with respect to the peak power for the windowed signals. Table 8 gives the ratio between the peak power and the mean power for binary and random phase reference functions for each of the four windows.

Applied window.	Binary pseudo-random function.	Random phase function.
Rectangular.	1.8	9.1
Hanning.	4.8	16.2
Blackman.	5.8	17.7
Blackman-Harris.	6.8	18.8

Table 8: Peak to mean power ratio for windowed reference functions.

The decrease in the mean power of the reference function under the tapered windows (i.e. Hanning, Blackman and Blackman-Harris) has resulted in a degradation in the process gain

and in the excision performance of the receiver. This is particularly noticeable for the random phase function where only the rectangular and Hanning windows show any improvement in excision performance between the carrier modulated and baseband systems.

This problem only exists within the hardware system used for the measurements, the simulated system had no such difficulties with the multipliers or the signal levels. Specific attention should be given to the despread multiplier in any further generation of the hardware demonstrator.

Chapter 5

5.1 A comparison of detection methods applied to binary and random phase functions.

Direct sequence spread spectrum modulation provides process gain against wide band noise for receivers that can generate a reference signal that is identical, and phase synchronised, to the transmitted spreading function. All other receivers are denied this process gain advantage, and are therefore unlikely to detect the transmissions (unless favourably located close to the transmitter) or to recover the data symbols. Conventional detection methods for Electronic Support Measure (ESM) receivers include the radiometer (which measures total energy within a given bandwidth) and the Panoramic Scanner (i.e. spectrum analyser). Both of these detection methods become very unreliable for signal to noise ratios close to 0 dB. Without knowledge of the spreading function, ESM receivers must attempt to exploit alternative methods to improve the signal to noise ratio and to extract as much information as possible from the received spread spectrum signal.

Important techniques include processor intensive applications such as high order statistical analysis [1], and simpler methods such as delay and multiply receivers. Because these techniques attempt to exploit the chipping structure of the binary pseudo random code, a random phase function may well be ideal for transmitters attempting to avoid detection. This chapter presents the results of simulations to compare the relative detection probabilities of binary and random phase codes by two detection methods;

i) delay and multiply receiver,
ii) spectral correlation technique.

The spectral correlation technique is based upon cyclostationary analysis presented by Gardner [2].

5.2 Delay and multiply ESM receiver.

A diagram of the delay and multiply process is shown in figure 34.

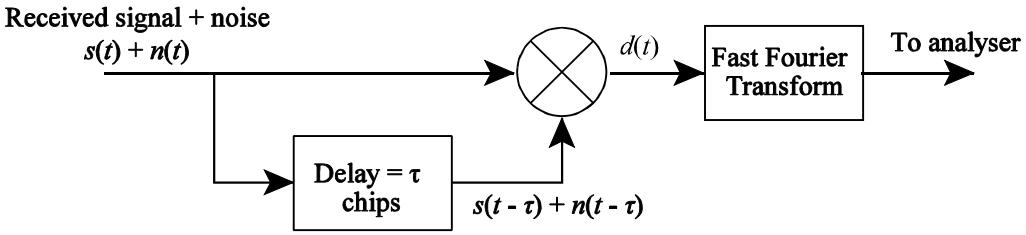

Figure 34 Delay and multiply detector.

With a delay, τ, of zero, the multiplier output at any time sample will be the square of the input voltage at that time sample:

$$d(t) = s^2(t) + n^2(t) + 2s(t)n(t).$$

where $s(t)$ is a wide bandwidth suppressed carrier signal with a centre frequency f_c, and $n(t)$ is

Gaussian distributed noise. Because there is no correlation between the noise $n(t)$ and the signal $s(t)$, the final term in the expression will represent wide band noise. The term $n^2(t)$ will represent wide band noise with a DC component, and $s^2(t)$ will form a spectral line at twice carrier frequency and at zero Hertz. Figures 35a) and b) show the spectrum at the input and output of the multiplier, with delay $\tau = 0.0$, a 64-chip binary sequence BPSK modulated on to a carrier (at FFT bin = 179) and with no added noise.

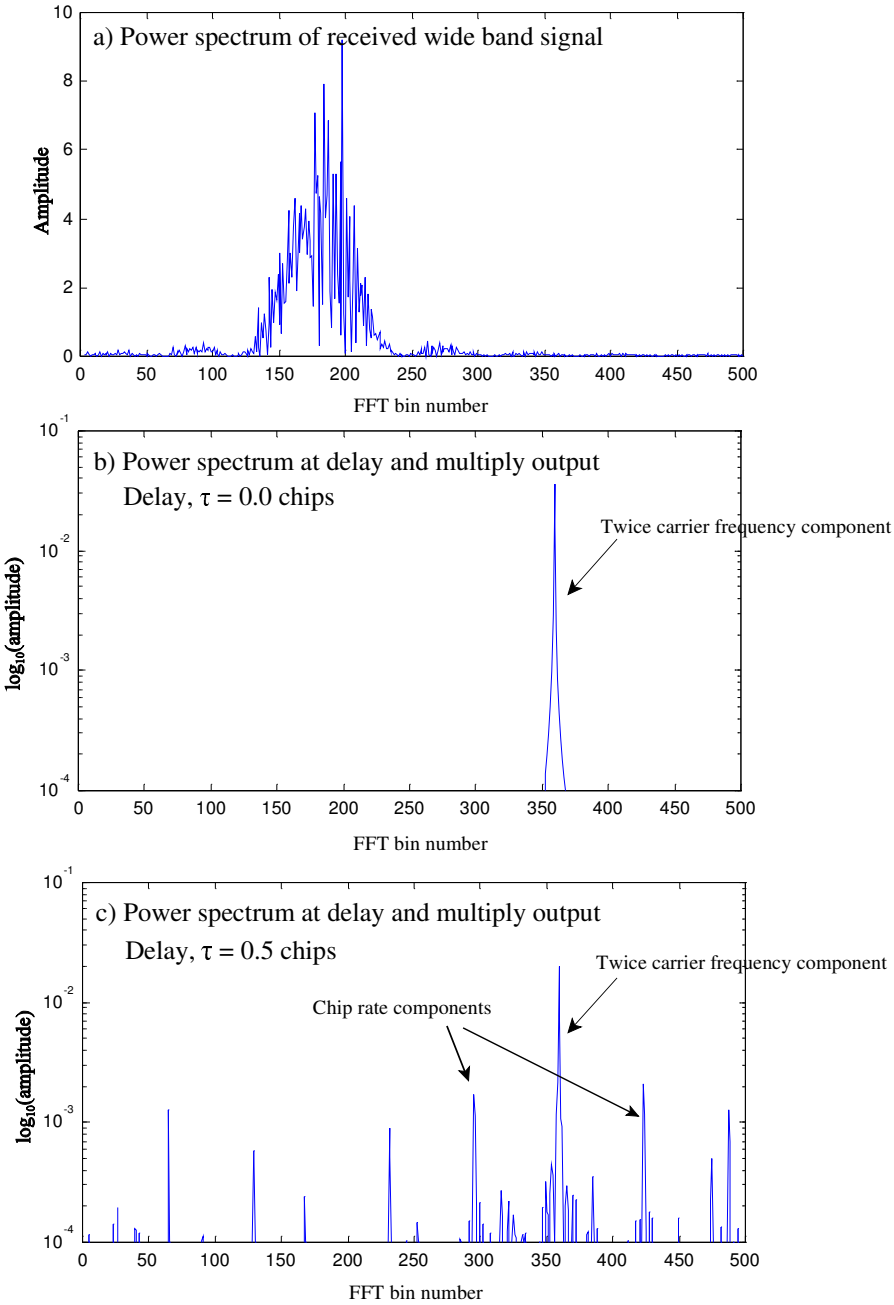

Figure 35 Power spectrum at input and output of delay and multiply detector.

When the delay, $\tau = 0.5$ chips, the power spectrum at the multiplier output will not only contain a frequency component at 2 x carrier frequency, but will also display frequency components at the code chip rate and associated harmonic frequencies. Figure 35c) shows the

output power spectrum

If the received signal to noise ratio is suitable, a delay and multiply ESM receiver may detect the component at twice carrier frequency, hence determining the true carrier frequency of the direct sequence signal. The chip rate components will reveal the code chipping rate. With Gaussian distributed noise added to the received signal, the probability of detection of the frequency components will depend upon the signal to noise ratio. Figure 34c) shows that the chip rate components have lower power than the twice carrier frequency term, and these would be the first to be lost as the signal to noise ratio decreases. Taking a number of successive Fourier transform blocks from the multiplier output, and averaging the result, will improve the detectability of the frequency components. However, the rate at which the probability of detection improves with the number of averaging blocks will decrease with falling SNR.

For all of the following simulations, a detection is declared as 'successful' if the frequency bin that contains the maximum power agrees exactly with the true carrier frequency, otherwise the detection is declared as 'unsuccessful'. The carrier frequency was changed randomly between each averaging run, and was dithered over the range 0 to 0.5 cycles per Fourier transform block in order to avoid artificially favourable detection conditions which will occur when there are an integer number of cycles in each block.

Figure 36 shows results for probability of detection of the twice carrier frequency component versus SNR and number of averaging blocks, for a binary pseudo-random code. Each Fourier transform block had 1024 samples and represented 64 chips. The delay offset $\tau = 0.0$ chips.

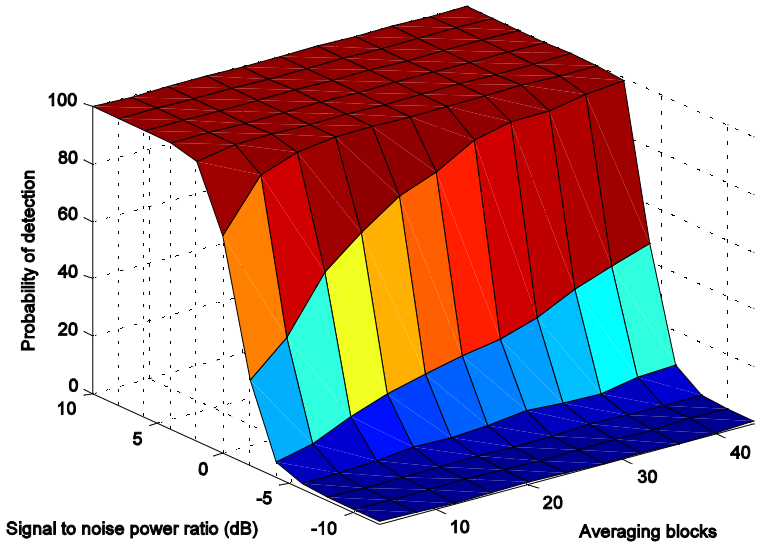

Figure 36 Probability of detection of twice carrier frequency component. Binary function. Delay and multiply detector, chip offset = 0.0 chip.

The maximum number of averaging blocks in the simulation was 44; the detection probability for this number is shown by figure 37a). It may be seen that the detection probability falls rapidly below -2 dB signal to noise ratio. This may be improved by 1 or 2 dB by increasing the number of averaging blocks and/or the Fourier transform block size.

Figure 37b) shows the probability of detection for the twice carrier frequency component when the detector delay is $\tau = 0.5$ chips. The detection probability is approximately 2 dB worse than for $\tau = 0.0$ chips. The magnitude of the chip rate components is approximately 2 dB lower than the twice carrier frequency component. However, once the signal has been initially detected the chip rate components could be revealed by more careful inspection. Initial detection should therefore be carried out with $\tau = 0.0$ chips, the delay then being optimised in an attempt to reveal any chip rate components.

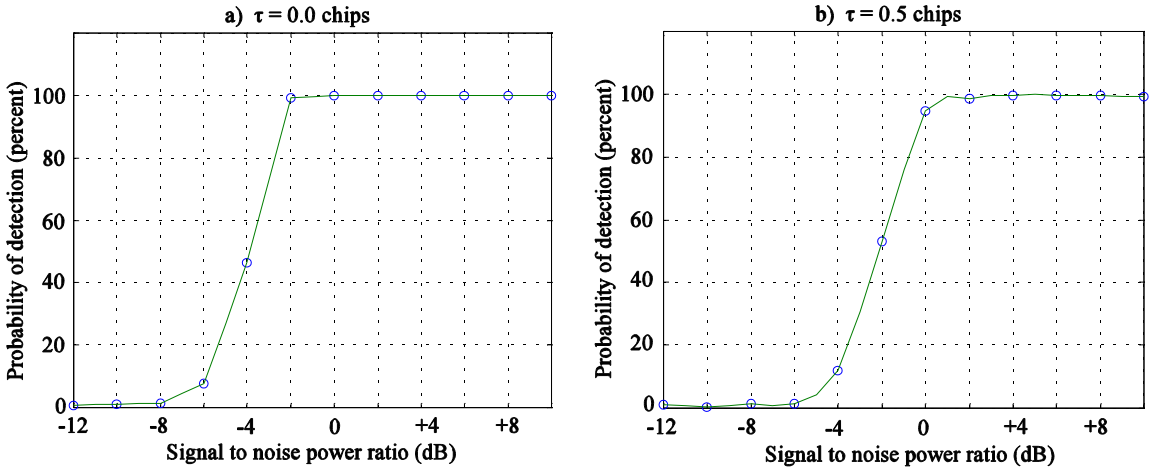

Figure 37 Probability of detection for delay and multiply detector.
Number of averaging iterations = 44.

For the random phase code under identical sampling conditions to those above, i.e. 1024 sample Fourier transform blocks, 64 bins set to unity magnitude (equivalent to 64 chips per block), the probability of detection for the twice carrier frequency component at $\tau = 0.0$ cycle offset is identical to figure 37a). Note that 1 cycle represents the highest frequency component in the main lobe, which is equivalent to the chip rate for a binary code. The random phase code has no chip structure, and with a delay offset of $\tau = 0.5$ cycles there are no isolated frequency components, hence the probability of detection is zero at this offset.

5.3 Sideband correlation ESM receiver.

Cyclic spectrum analysis, which combines frequency samples within a Fourier transform block, was presented by Gardner [2]. Consider a sampled time domain signal $x(t)$, with sample values $x(nT_s)$ having N samples with sampling interval T_s seconds. The Fourier transform is given by:

$$X_T(f) = \sum_{n=0}^{N-1} x(nT_s) e^{-j2\pi \frac{nm}{NT_s}} \quad \ldots . (1)$$

Where T represents the total duration of the time window, $T = NT_s$.

Cyclic spectrum analysis forms the relationship:

$$S_{xT}^{\alpha}(f)_{\Delta f} = \frac{1}{M+1} \sum_{m=-\frac{M}{2}}^{\frac{M}{2}} S_{xT}^{\alpha}\left(f + \frac{m}{NT_s}\right) \ldots . (2)$$

where:

$$S_{xT}^{\alpha}(f) = \frac{1}{N} X_T\left(f + \frac{\alpha}{2}\right) X_T^*\left(f - \frac{\alpha}{2}\right) \ldots . (3)$$

Equation 3 represents the complex product of two frequency samples, spaced at $\pm\frac{\alpha}{2}$ about a centre frequency f, and where the superscript * denotes the complex conjugate. Equation 2 forms the sum of the complex product with α fixed, over a range, M, of frequency bins. Figure 38 illustrates the concept.

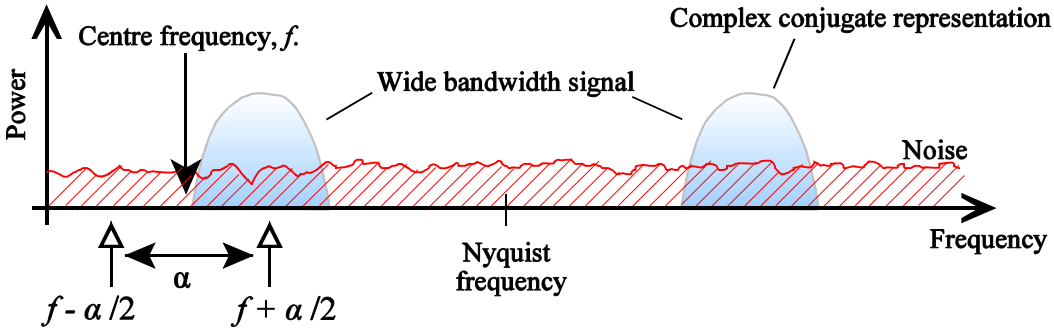

Figure 38 Illustrating the relationship between centre frequency, f, and spacing, α.

Figure 39 represents a plot of equation 2 for a 63 chip m-sequence, binary PSK modulated on to a carrier with a frequency of twice the chip rate and with no added noise.

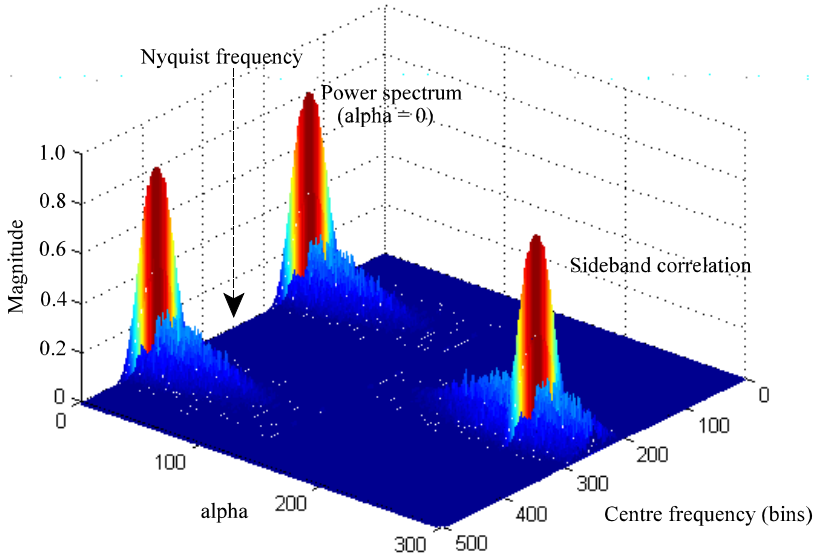

Figure 39 Cyclostationary surface.

For figure 39, $x(t)$ was sampled at 8 samples per chip, hence each Fourier transform block consisted of 504 samples. The Nyquist sample rate was represented by sample number 252.

When $\alpha = 0$, the cyclic spectrum analysis forms the frequency-power spectrum of the signal $x(t)$. For α greater than 0 but less than Nyquist the algorithm calculates the spectral cross-correlation averaged over a window of size M. Frequency samples representing Gaussian noise will have no relationship to each other for $\alpha > 0$ and will tend to average toward zero as the window size M becomes very large. Figure 40 represents the cyclic spectrum surface when $x(t)$ is purely Gaussian noise and $M = 24$ samples.

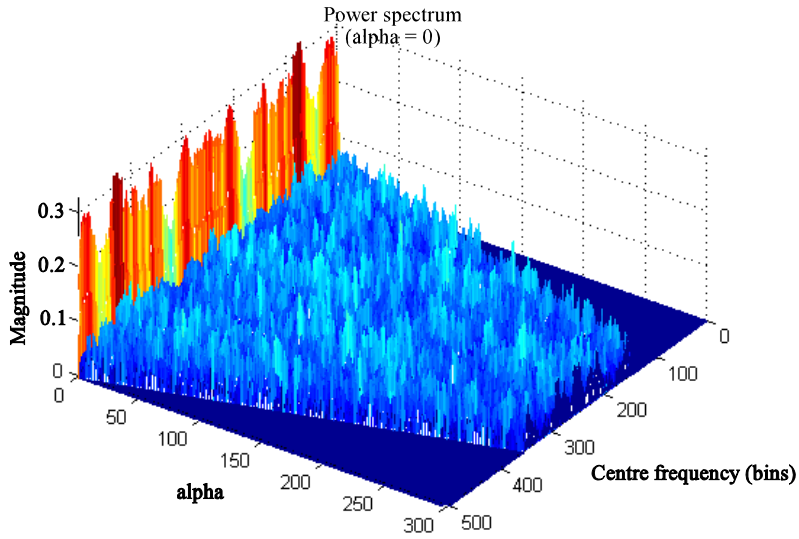

Figure 40 Cyclostationary surface when $x(t) = n(t)$.

When α = Nyquist, the cyclic spectrum forms the correlation between the two sidebands of the modulated signal (figure 41).

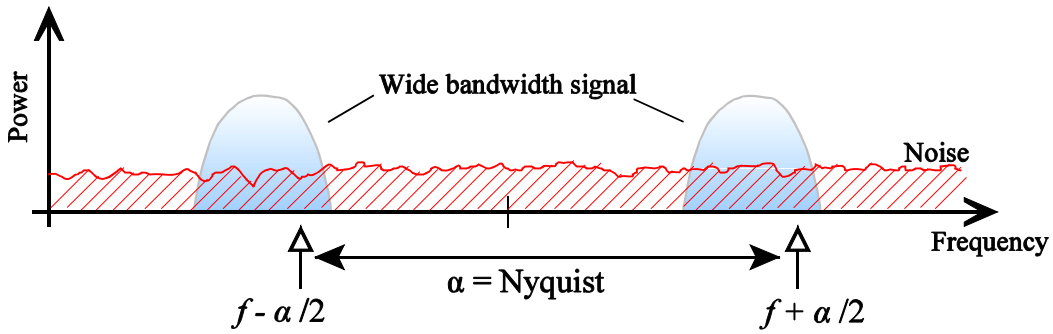

Figure 41 Spectrum samples when α = Nyquist.

The peak located at α = Nyquist in figure 39 represents the relationship between the two sidebands which, for BPSK modulation, are the complex conjugate of each other. Figure 42 shows the cyclic spectrum surface when $x(t)$ consists of a BPSK modulated 63 chip m-

sequence with AWGN such that the signal to noise ratio = 0 dB, and the window size $M = 24$.

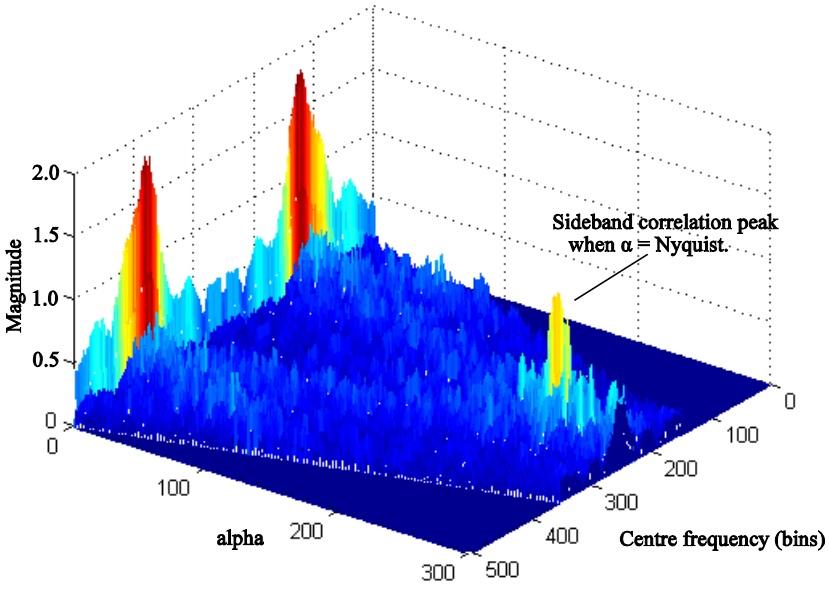

Figure 42 Cyclostationary surface. BPSK modulated 63 chip m-sequence, 0 dB SNR.

For signal detection it is only necessary to calculate the sideband correlation; all other parts of the surface add no further information. The algorithm may be modified to reduce the amount of computation and to concentrate only on the correlation between the two sidebands; figure 43 and equations 4 and 5 illustrate the modified approach.

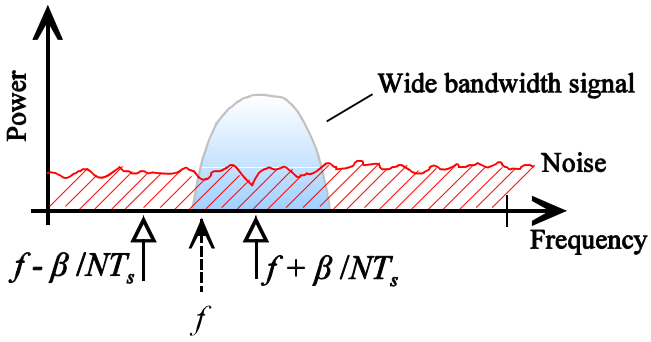

Figure 43 Modified algorithm for signal detection.

$$S_{xT}(f)_{\Delta f} = \frac{1}{MN}\sum_{\beta=1}^{M} X_T\left(f + \frac{\beta}{NT_s}\right) X_T\left(f - \frac{\beta}{NT_s}\right) \quad \ldots\ldots (4)$$

$$X_T(f) = \sum_{n=0}^{N-1} x(nT_s)\, e^{-j2\pi \frac{nm}{NT_s}} \quad \ldots\ldots (5)$$

Only the below-Nyquist part of the frequency spectrum is required, and as there is only one independent variable involved (the centre frequency f, as the averaging window size M remains constant) the correlation magnitude $S_{xT}(f)_{\Delta f}$ may be plotted on a two dimensional graph. Figures 44 and 45 show the frequency/power spectrum and correlation magnitude for a BPSK modulated 63 chip m-sequence with no added noise and with signal to noise ratio = 0 dB, respectively.

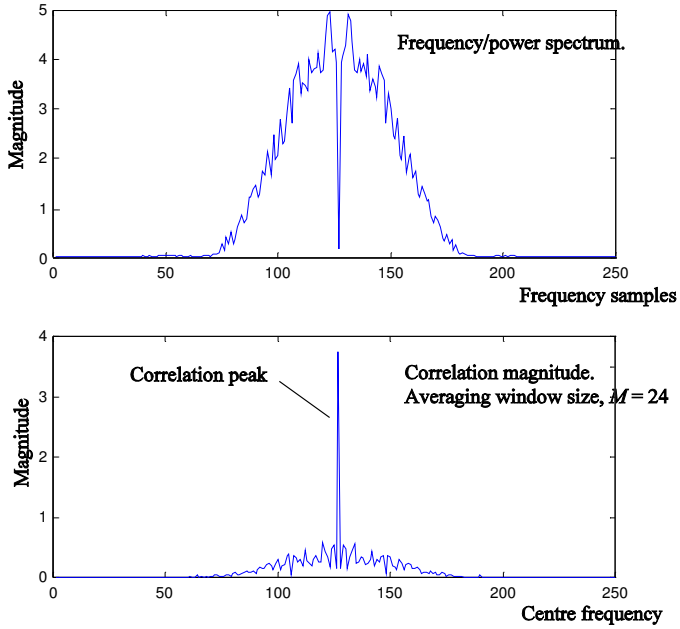

Figure 44 Spectral correlation. 63 chip m-sequence, 8 samples/chip, no added noise.

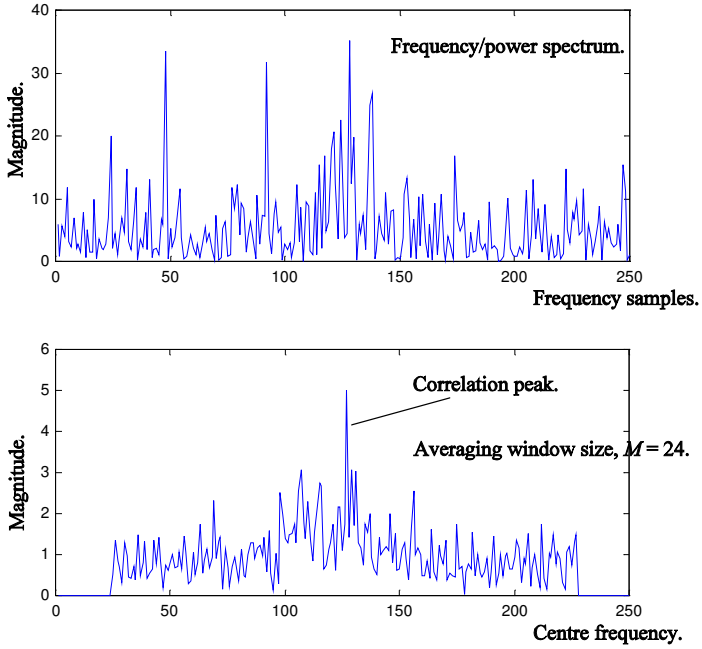

Figure 45 Spectral correlation. 63 chip m-sequence. SNR = 0 dB.

Note that the correlation peak coincides with the carrier frequency, hence detection of the wide-band signal reveals the carrier frequency but provides no information as to the chipping rate of the function.

The averaging window size, *M*, must be optimised for maximum detection probability. *M* will be dependent upon the bandwidth of the wide band signal. Figure 46 shows the probability of detection versus signal to noise ratio (with added white Gaussian noise) and *M*, for a BPSK modulated binary spreading function with a Fourier transform block size of 64 chips from a 255 chip m-sequence. From this figure the optimum value for *M* is shown to be a function of SNR.

$$M_{opt} = 2.5 \times SNR(\text{dB}) + 44.0 \text{ bins} \quad \ldots\ldots (6)$$

The fact that the optimum window size is a function of SNR is to be expected for a function with a non-flat spectral distribution, such as a binary sequence.

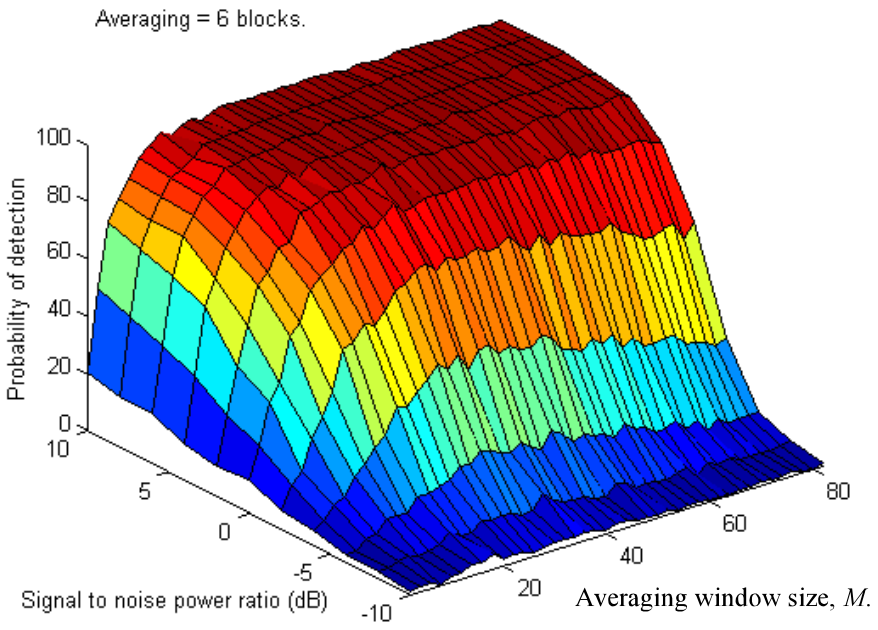

Figure 46 Probability of detection for binary PN code.
Six averaging iterations per detection.

As earlier (see section 5.2), a detection is assumed to be true if the maximum detected peak agrees exactly with the known carrier frequency, otherwise the 'detection' is false. A number of successive blocks are averaged in order to improve the detection probability; in plotting figure 46 each detection attempt averages six blocks.

The probability of detection will improve by increasing the number of averaging blocks. However, the rate of improvement rapidly decreases as the signal to noise ratio becomes lower. Figure 47 shows probability of detection versus the number of averaging blocks and signal to noise ratio, for the optimum window size given by equation 6. Figure 48 plots the probability of detection versus SNR when using 44 averaging block per attempt. This may be directly compared with figure 37 for the delay and multiply detector.

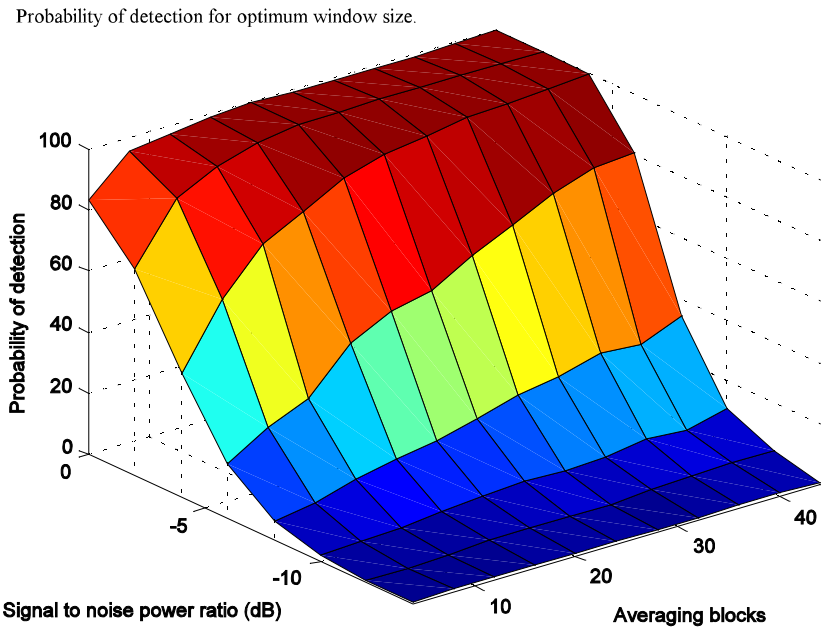

Figure 47 Probability of detection. Binary PN code with 64 chip blocks from 255 chip sequence. BPSK modulation.

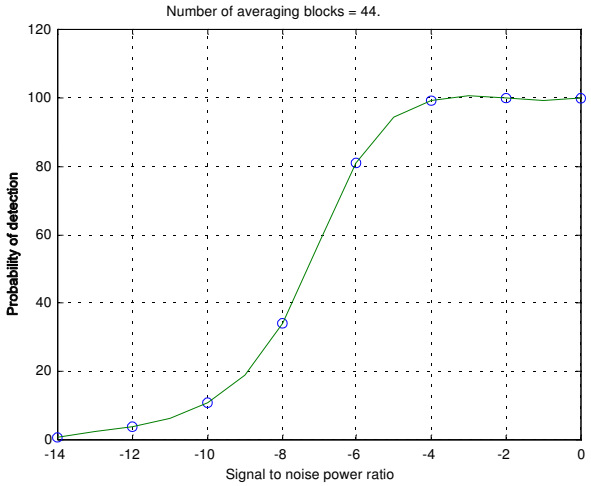

Figure 48 Probability of detection with optimum window size, number of averaging blocks = 44. Binary spreading function.

The random phase function has a flat frequency versus power spectrum. For a spreading function with 64 bins each of random phase and unity magnitude, tests show that the optimum window size is 64 bins, and is independent of signal to noise ratio. The probability of detection versus SNR with 44 averaging blocks per attempt, is shown by figure 49. This is almost identical to figure 48.

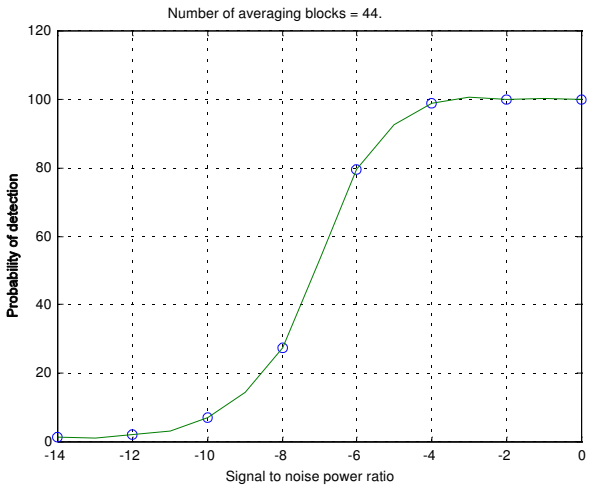

Figure 49 Probability of detection with optimum window size, number of averaging blocks = 44. Random phase spreading function.

5.4 Discussion.

Chapter 5 has presented two methods for the detection of carrier modulated wide band spread signals which are received with signal to noise ratios of less than 0 dB. Each method is trialed in its ability for detecting binary spreading functions and random phase spreading functions. The delay and multiply ESM receiver has a poorer probability of detection than the spectral correlation method, but is capable of providing information on the code chip rate of binary spreading functions. A random phase function can only be detected by a delay and multiply receiver for delay offsets of zero.

The spectral correlation method has been shown by simulation to provide detection probabilities of 80% for signal to noise ratios down to -6dB, for block lengths of 64 chips (or equivalent for the random phase function). The detection performance is unaffected by the type of spreading function.

The spectral correlation method has only been investigated for binary PSK modulated signals, where both sidebands are closely related, i.e. they are complex conjugate mirror images. Further work is required to develop this method for the detection of signals with quadrature (or higher) PSK modulation.

Chapter 6

6.1 Conclusions.

A wide band, spectrally flat spreading function follows naturally when generation is by fast Fourier transform from a frequency domain specification. This analogue noise-like signal differs from the time domain specified spreading functions normally selected for direct sequence spread spectrum systems, and can offer some advantages when applied to communication transmissions that are required to be covert and to be tolerant of deliberate interference. The most significant problem associated with a random phase function lies in its wide dynamic range. Such signals are difficult to transmit efficiently, although this has not prevented the widespread adoption of orthogonal frequency division multiplex (OFDM) transmissions for civil radio networks. Commercial development of OFDM has lead to the development of hardware for real-time FFT generation of wide bandwidth signals, and to the transmission of high-power noise-like signals with a wide dynamic range. Direct sequence spreading has traditionally used wide bandwidth signals generated by time domain algorithms; the resulting spectrum often being less than ideal for the application. There is now the possibility of directly defining the signal spectrum of a direct sequence system in response to channel conditions in order to:

a) minimise the damage caused by intentional interference,
b) minimise the interference to narrow band co-channel users from the direct sequence transmissions, and
c) minimise the probability of detection by ESM receivers of covert spread spectrum transmissions.

This report has addressed points a) and c), and comes to the following conclusions:

The technique of placing spectral nulls within the reference function can provide effective excision of narrow band interference in a direct sequence spread spectrum receiver. Coupling spectral nulls with appropriate time domain windowing has been shown to provide excision levels of up to 25 dB by first generation hardware, and in excess of 100 dB by simulation.

The random phase function has, at best, only a marginal advantage over a binary pseudo-random function for the excision of swept-frequency narrow band interferers. However, the constant power versus frequency relationship within the main lobe of the random phase function can provide an excision advantage of at least 3 dB over the pseudo-random function for interferers located close to the carrier frequency. This is at the expense of poorer excision (of at least 7 dB) for interferers with a frequency close to the edge of the main lobe. (See figures 29 and 30).

ESM receivers must normally cope with a signal to noise ratio below 0 dB. and without knowledge of the spreading function used by the direct sequence transmitter. Sophisticated detection and analysis methods, such as high order statistical analysis [1], can target the chipping structure of binary pseudo-random functions. Simpler approaches, such as the delay and multiply receiver, rely on enhancing the frequency components at the chipping rate. A random phase function has no chipping structure

that may be exploited and would therefore be undetectable by these methods. However, against energy level detectors (i.e. squaring detectors and radiometers) or techniques that exploit relationships between the sidebands of a modulated signal (cyclo-stationary analysis), a random phase function has been shown to provide no advantage over a binary pseudo-random function.

Non-binary spreading functions for jamming excision in direct sequence spread spectrum systems has been researched by other workers [3]. Wavelet analysis may be used to isolate and remove that part of the spread signal bandwidth where the jammer to signal power ratio (JSR) exceeds a pre-determined threshold. Results quoted consider SJR's in the range 10 dB to 30 dB, and show improvements of approximately 10 dB over the non-excised condition.

6.2 Further work.

This report has considered the use of reference code spectral shaping to excise narrow band interferers from direct sequence spread spectrum receivers. Although the only deliberate interference considered has been a swept-frequency sinusoid, the technique would be equally comfortable with narrow band noise-modulated jammers and multiple jamming tones.

The computer simulations have proved useful in selecting optimum parameters, such as notch width and window type, and of showing the levels of excision that would be achievable. However, simulations must eventually be translated into practical hardware and this is often where the problems begin. The time spent developing the hardware demonstrator and taking results has been considerable, but the experience gained has provided a useful foundation on which to base any succeeding practical test-bed.

If jammer excision alone is to be an end goal, then this work has shown the possibilities of spectral shaping using conventional binary pseudo-random spreading functions. The spectrally shaped pseudo-random codes may be generated via an inverse Fourier transform from a frequency specification, in which case further work would be required to explore code generation in this way, or may be generated using conventional time domain methods and then shaped via FFT/IFFT processing. If random phase spreading functions are to be considered then further work should include reduction of the dynamic range of the function without compromising the spectral shape, code division multiple access performance and the advantages gained by using spectrally flat wide band functions in a multipath environment.

References.

1. E R Adams, “Identification of pseudo-random sequences in DS/SS intercepts by higher-order statistics”. Sponsored by Sensors Directorate (USAF), WPAFB, Dayton, Ohio. Reference: 014032.

2. W A Gardner, “Signal interception: a unifying theoretical framework for feature detection”. IEEE Transactions on Communications, 1988, volume 36, pages 897-906.

3. Y Zhang, J Dill, “An anti-jamming algorithm using wavelet packet modulated spread spectrum”. IEEE proceedings MILCOM 1999, volume 2, pages 846-850.

Appendix 1

Further graphical results from the baseband simulation.

1.1 Notch width versus jammer frequency (Section 2.2.2, page 9).

These curves of bit error probability with the jammer at a range of fixed frequencies across the spectrum of the wide band function and with null widths from 2 to 60 bins, show the following results:

1) The width of the excision null for minimum bit error probability does not depend upon the frequency of the jammer.
2) For the random phase function, the bit error probability is largely unaffected by the jammer frequency, but for the binary pseudo-random function the bit error probability is affected by the jammer frequency.
3) The plots for the binary pseudo-random function are uneven, showing that there are 'vulnerable' frequencies due to the uneven distribution of the power across the spectrum. These plots should be compared to those for the random phase function.

1.1.1 Binary pseudo-random function.

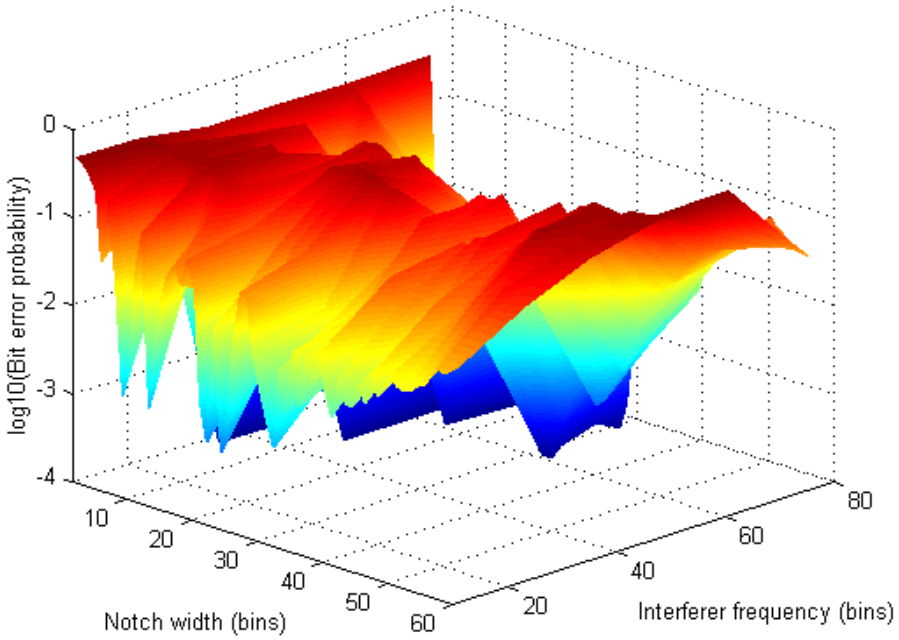

Figure 1 Rectangular window. SNR = +12.0 dB, SJR = -20.0 dB.

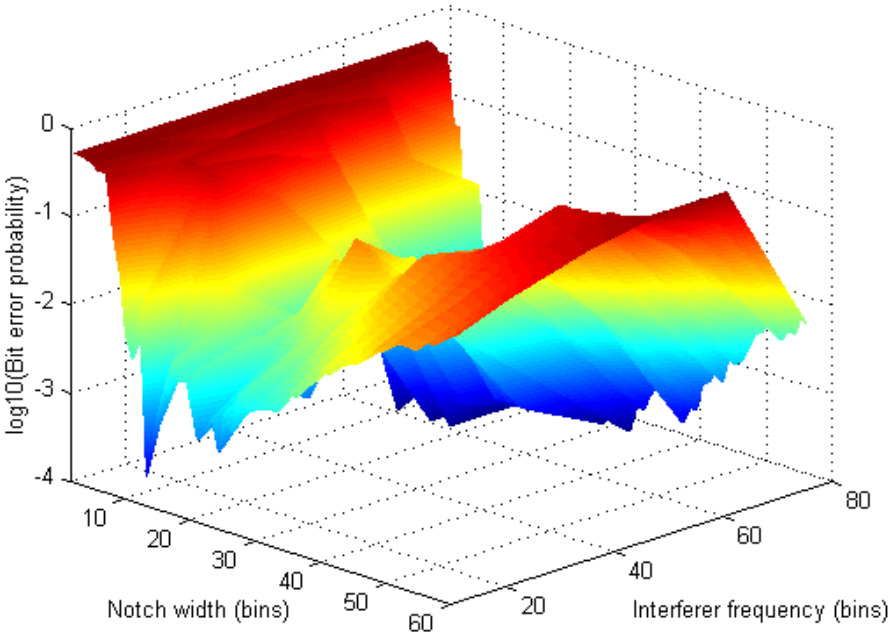

Figure 2 Hanning window. SNR = +12.0 dB, SJR = -64.0 dB.

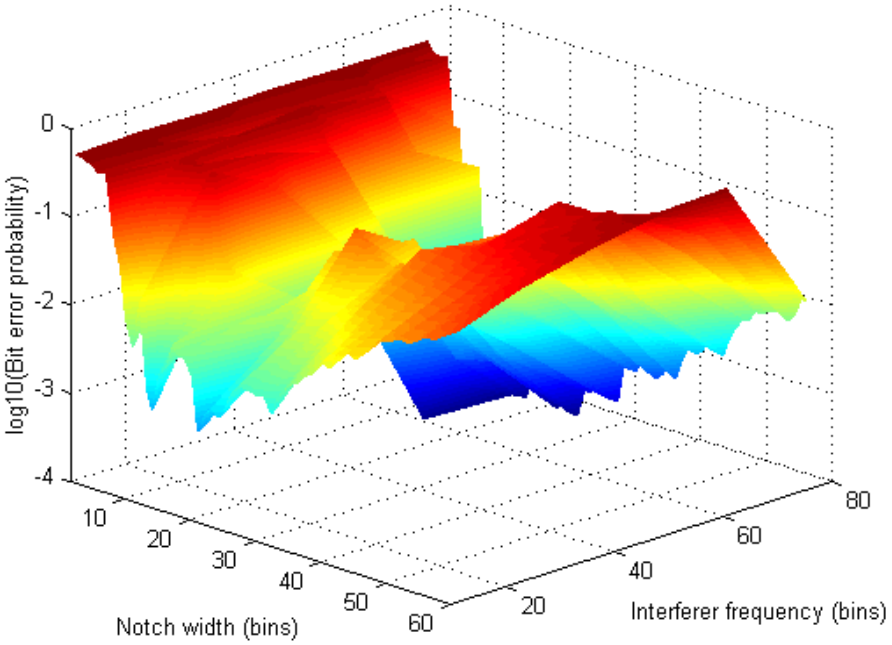

Figure 3 Blackman window. SNR = +12.0 dB, SJR = -72.0 dB.

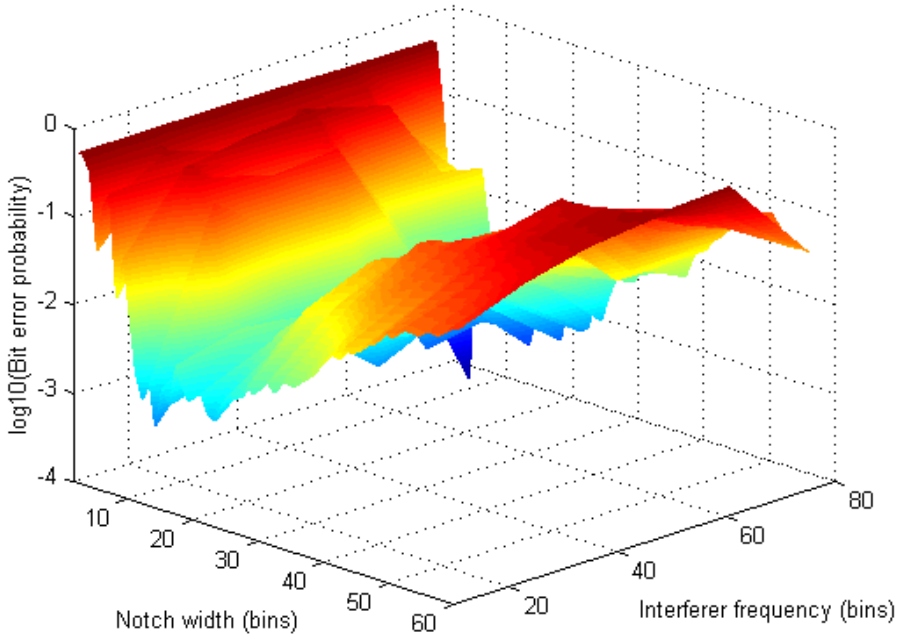

Figure 4 Blackman-Harris window. SNR = +12.0 dB, SJR = -90.0 dB.

1.1.2 Random phase function.

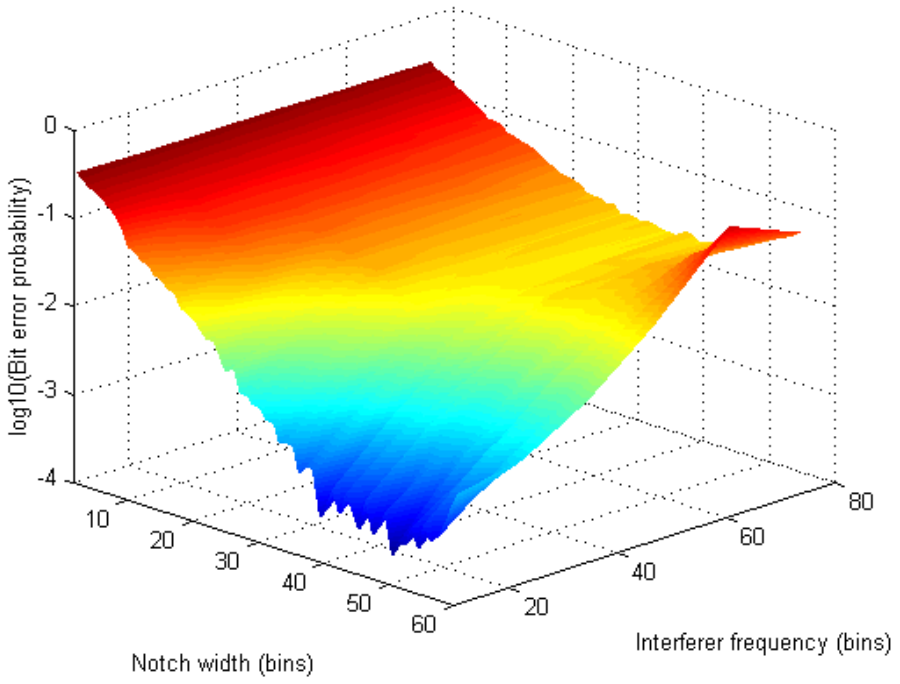

Figure 5 Rectangular window. SNR = +12.0 dB, SJR = -20.0 dB.

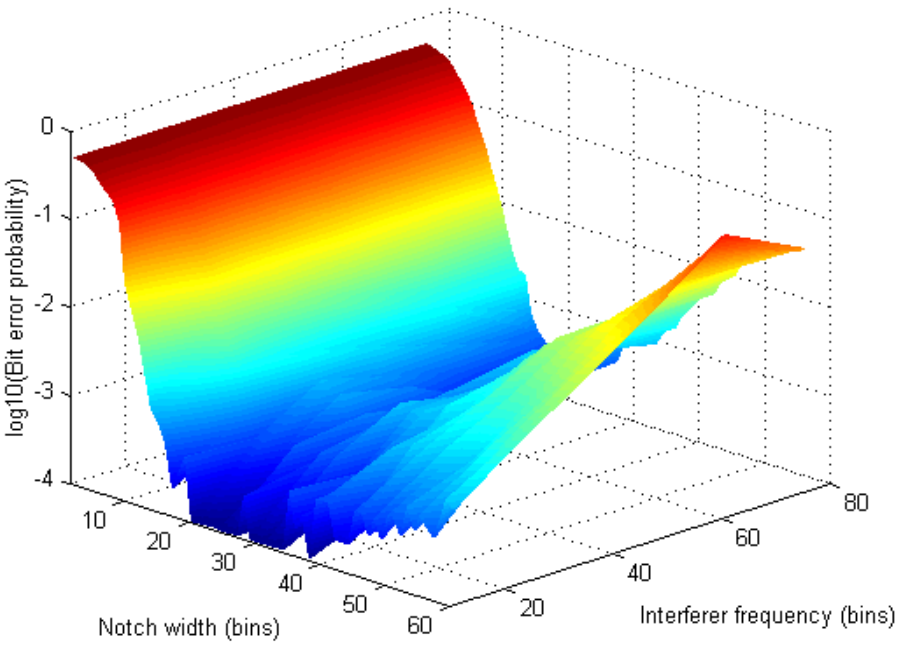

Figure 6 Hanning window. SNR = +12.0 dB, SJR = -64.0 dB.

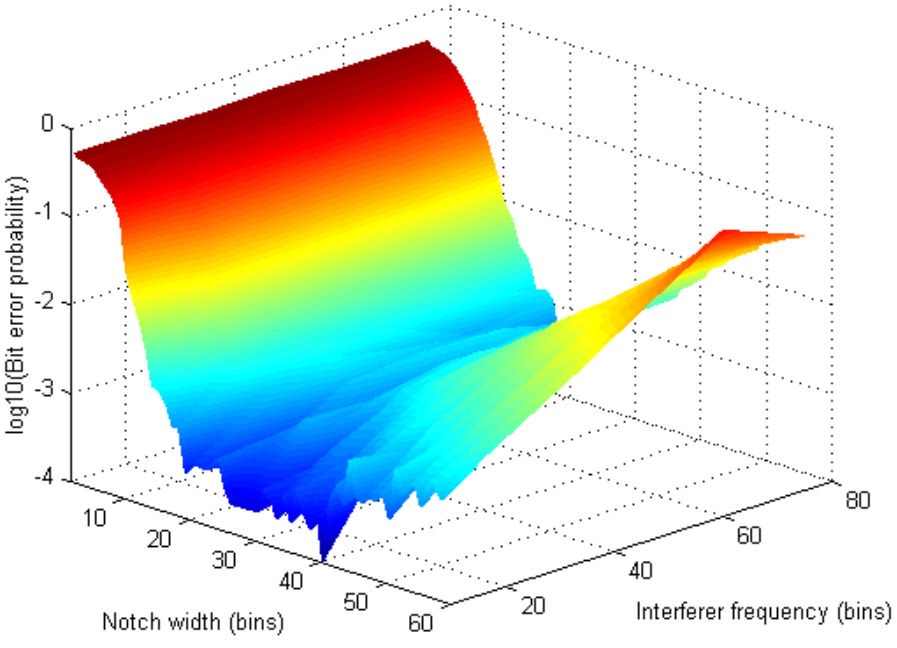

Figure 7 Blackman window. SNR = +12.0 dB, SJR = -72.0 dB.

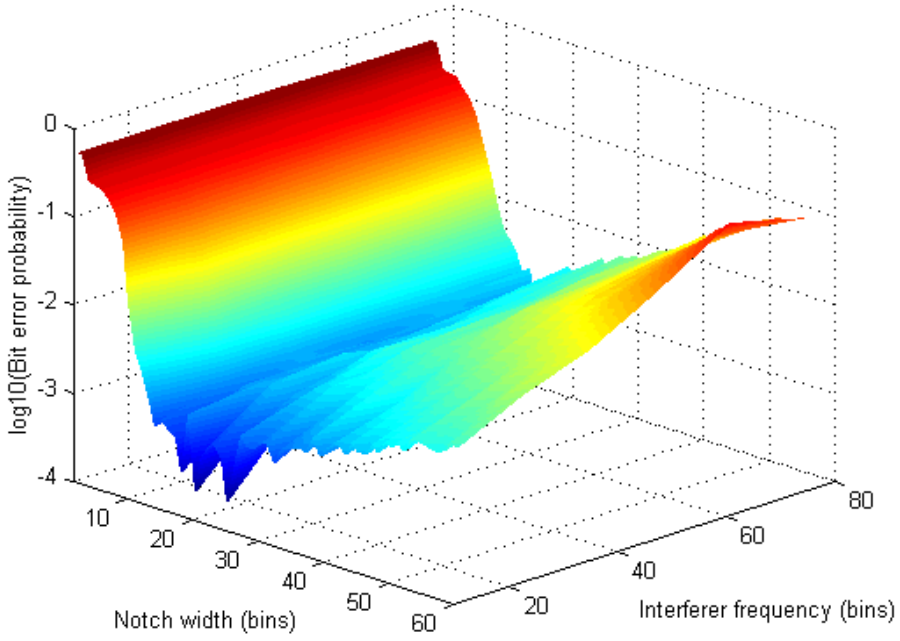

Figure 8 Blackman-Harris window. SNR = +12.0 dB, SJR = -90.0 dB.

The excision null is truncated at zero frequency, removing less of the energy from the wide band reference. Hence the reduction in bit error probability as the jammer frequency approaches zero Hertz. This effect is particularly noticeable in figure 5, for the random phase function with rectangular window.

1.2 Notch width versus signal to jammer power ratio (Section 2.2.1, page 7).

Increases in null width will improve the level of jammer excision, but reduce the process gain to white Gaussian noise. There will be an optimum null width where any further increase will degrade the bit error probability. These simulated results use a jammer with its frequency swept across the spectrum of the wide band function, and with a range of signal to jammer power ratios, to determine the optimum null width.

In each case the signal to noise ratio was fixed at value to give a minimum bit error probability of approximately 10^{-3}.

In the following graphs, the signal to jammer power ratio is in dB's.

1.2.1 Binary pseudo-random function.

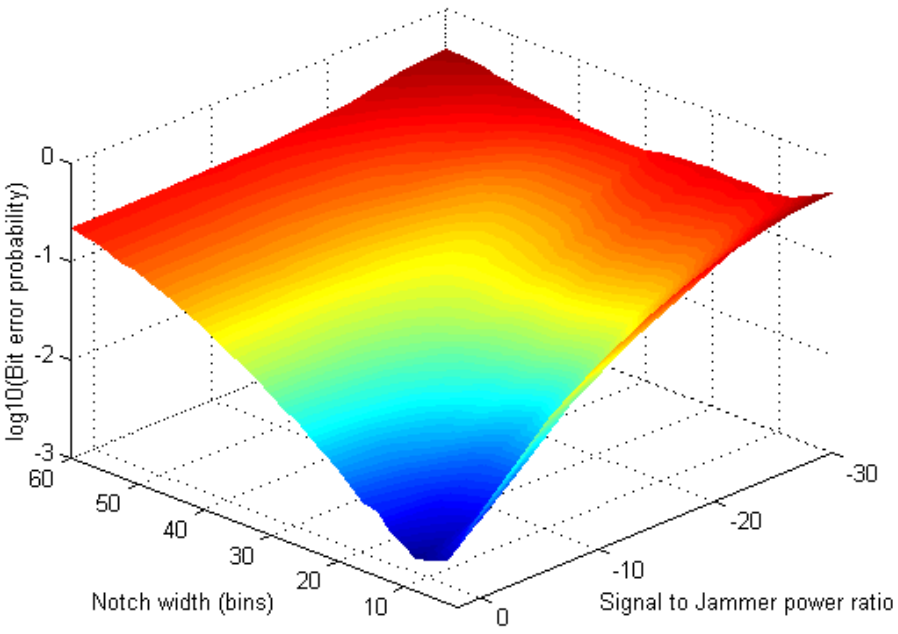

Figure 9 Rectangular window. SNR = +7.0 dB.

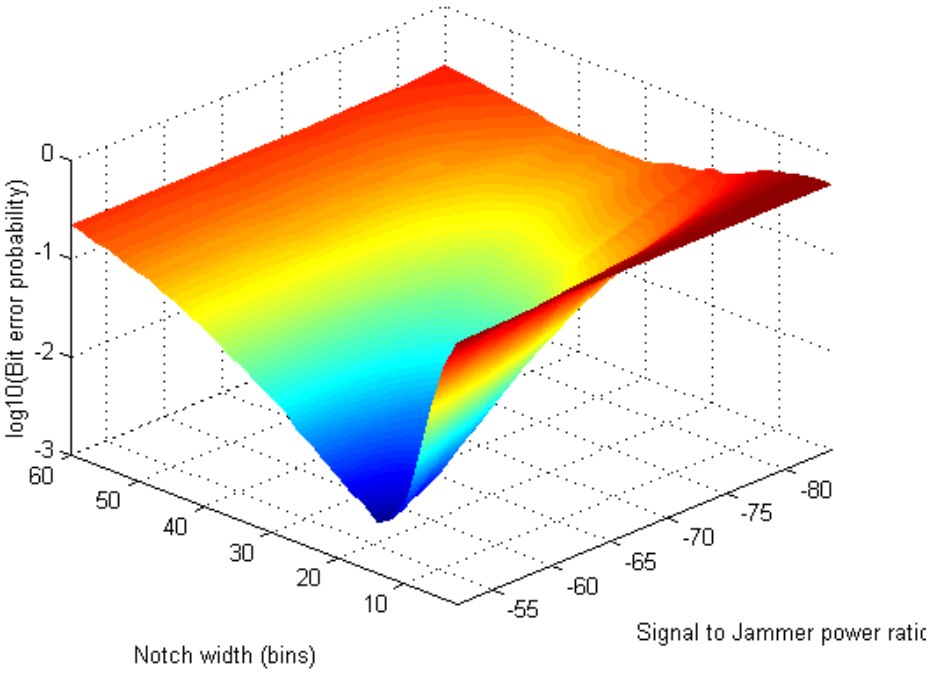

Figure 10 Hanning window. SNR = +9.0 dB.

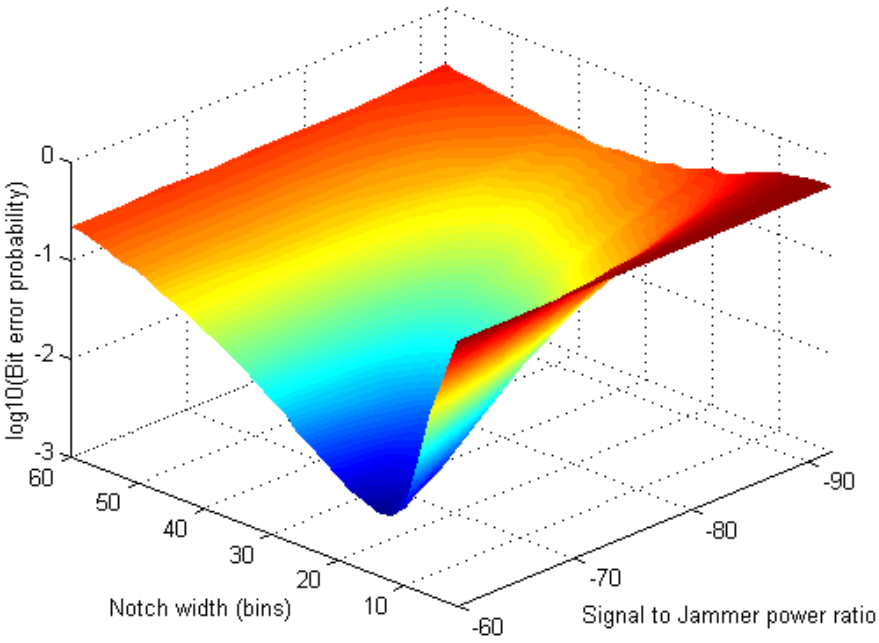

Figure 11 Blackman window. SNR = +9.5 dB.

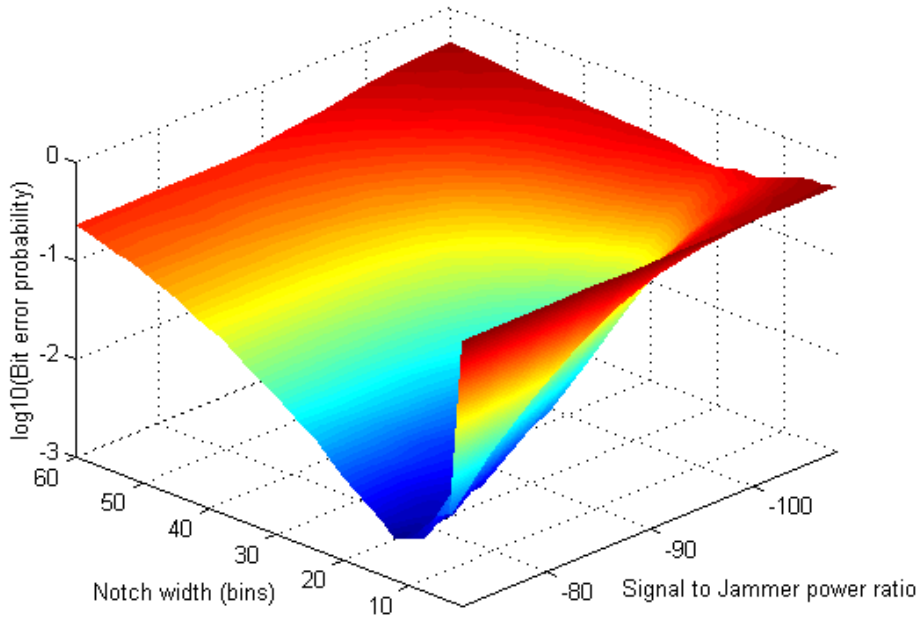

Figure 12 Blackman-Harris window. SNR = +10.0 dB.

1.2.2 Random phase function.

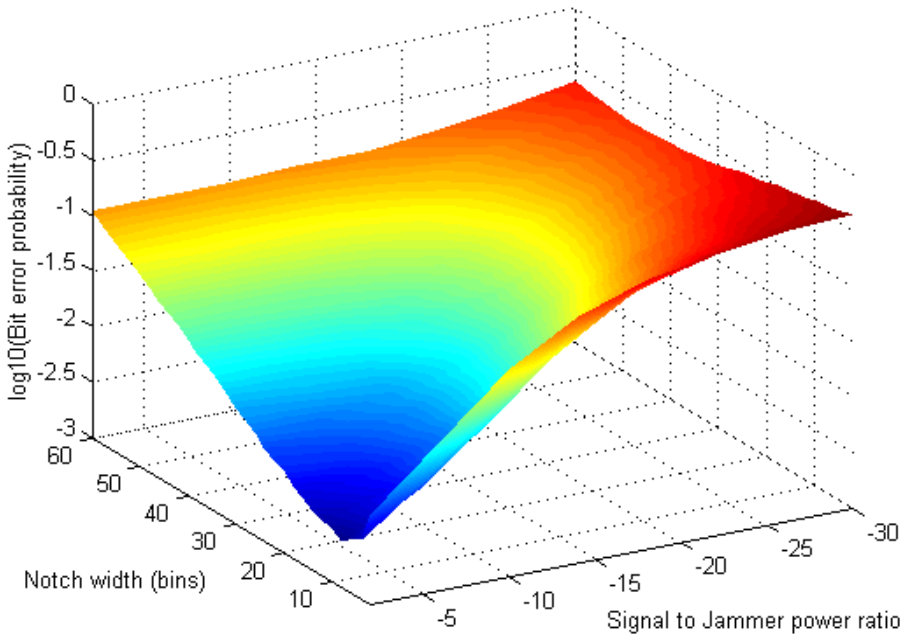

Figure 13 Rectangular window. SNR = +7.0 dB.

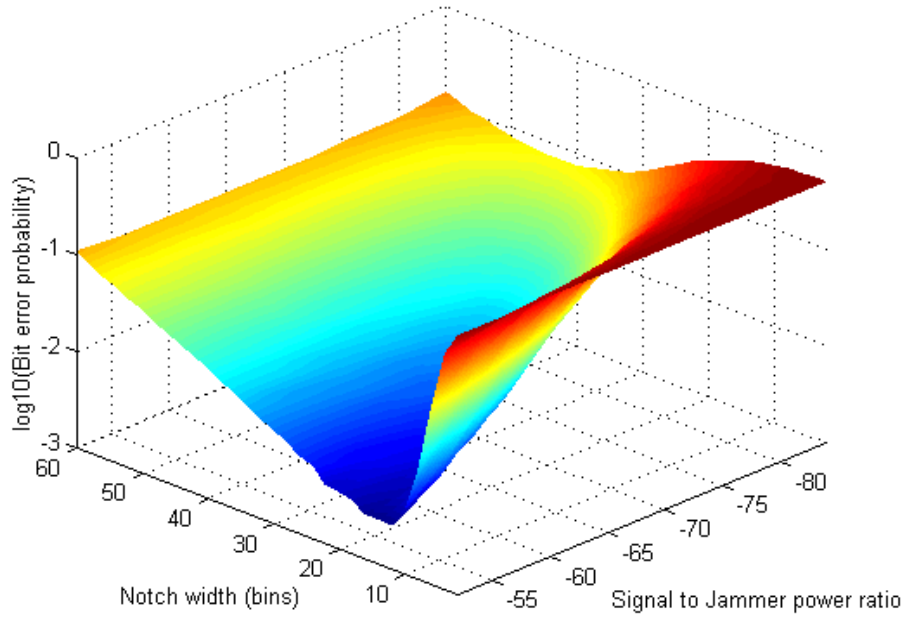

Figure 14 Hanning window. SNR = +9.0 dB.

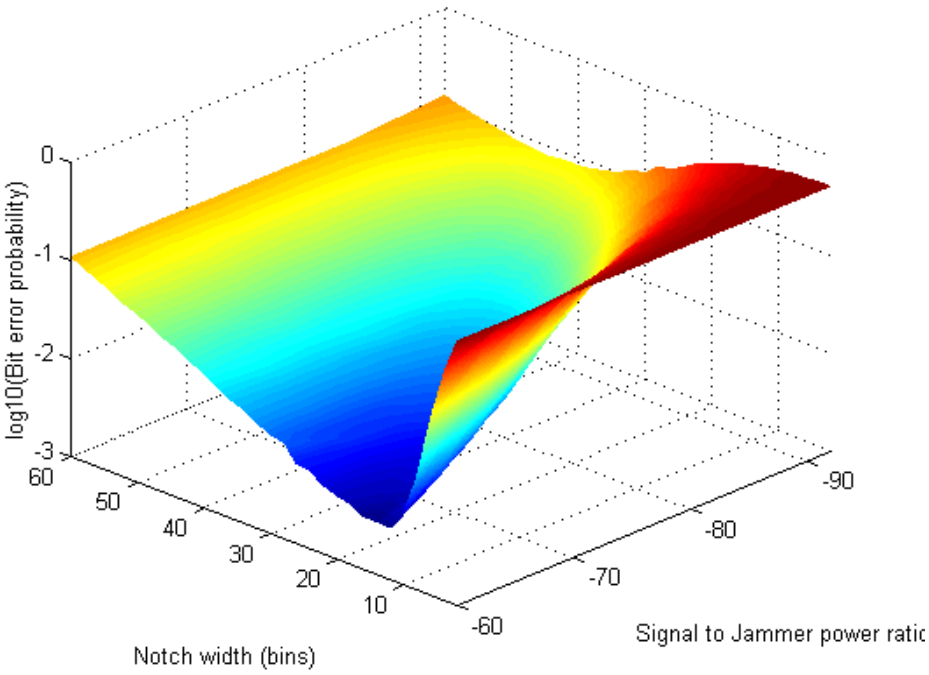

Figure 15 Blackman window. SNR = +9.5 dB.

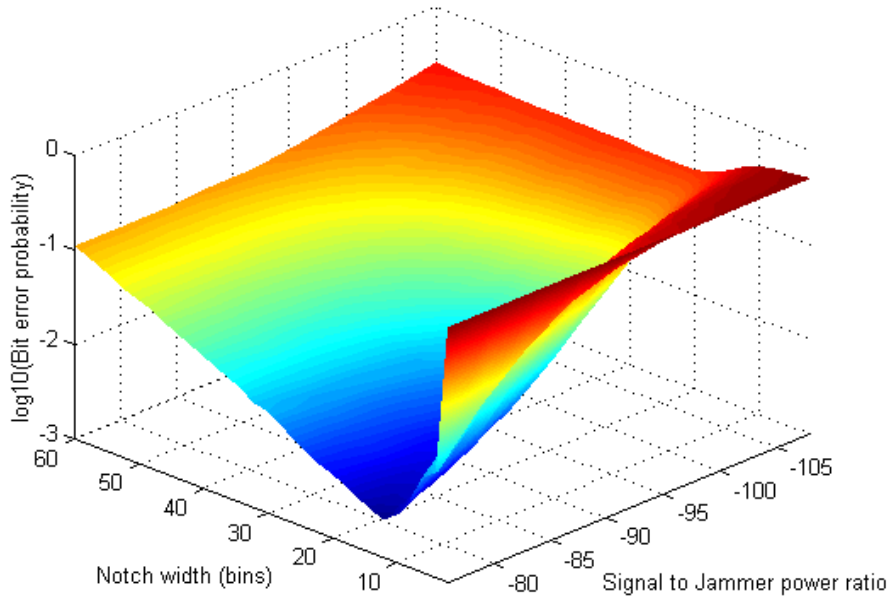

Figure 16 Blackman-Harris window. SNR = +10.0 dB.

1.3 Excision results, using optimum notch width. (Section 2.4, page 12).

These curves Compare the bit error probability versus signal to jammer power ratio for the excised and non-excised systems. The jammer was swept in frequency across the bandwidth of the wide band function. In all cases the signal to noise power ratio remained fixed at +12.0 dB.

1.3.1 Binary pseudo-random function.

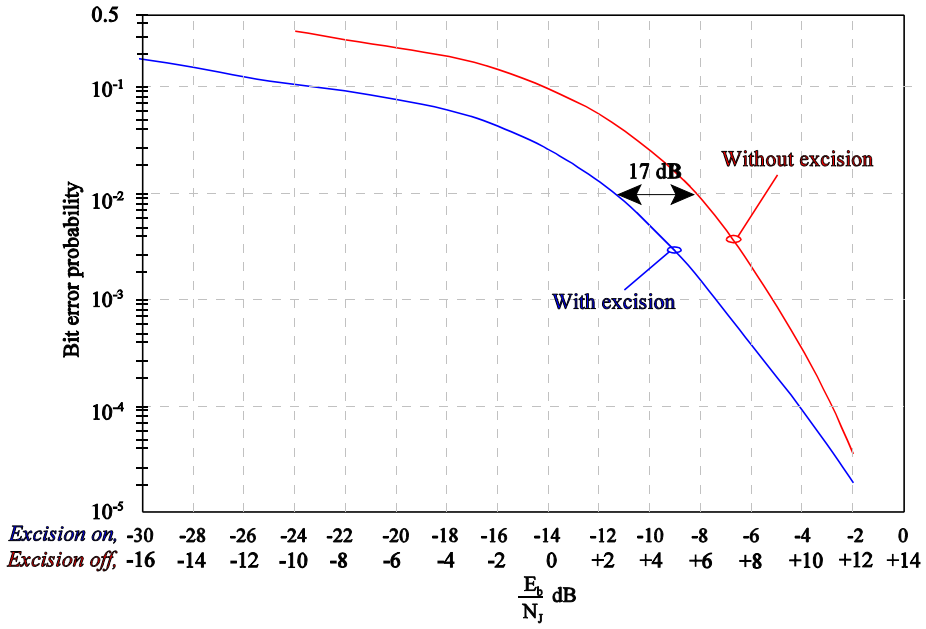

Figure 17 Rectangular window.

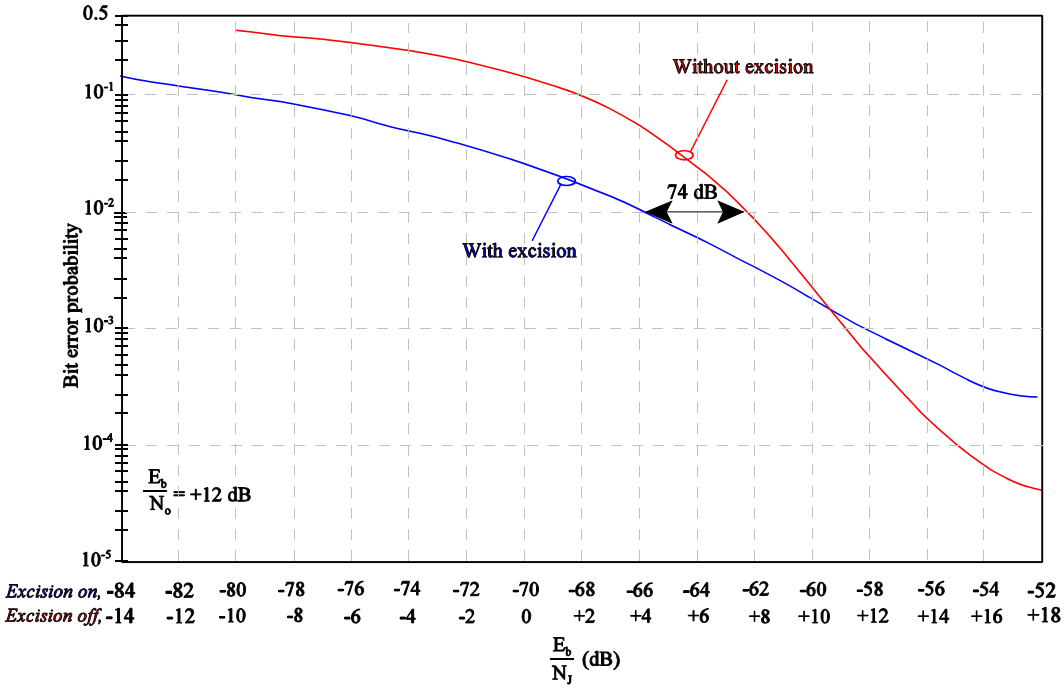

Figure 18 Hanning window.

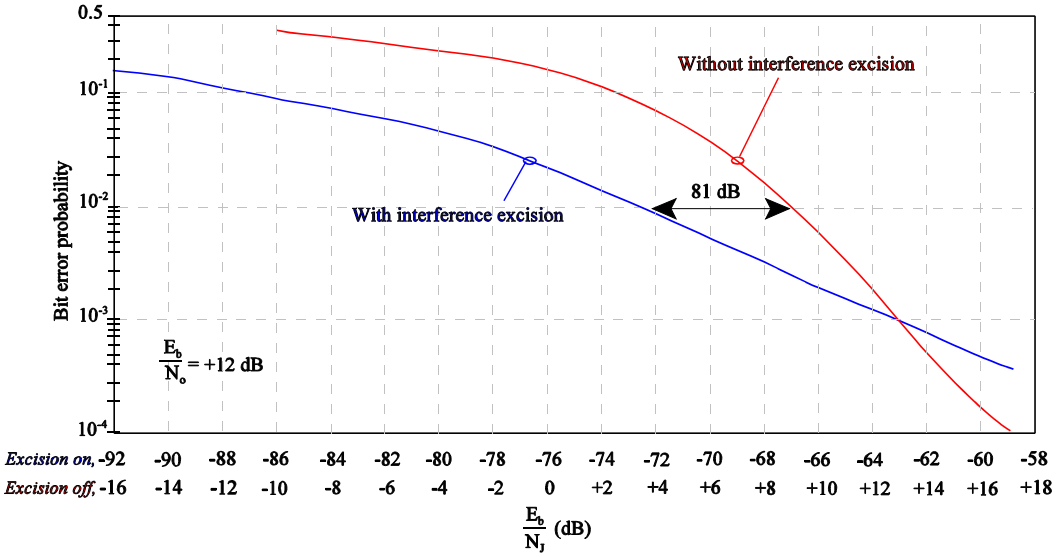

Figure 19 Blackman window.

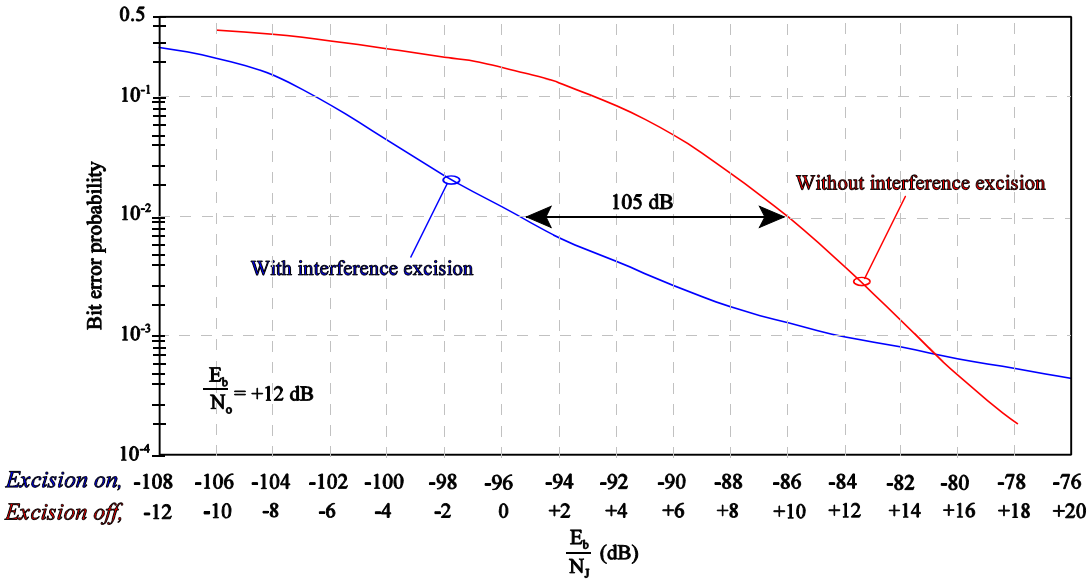

Figure 20 Blackman-Harris window.

1.3.2 Random phase function.

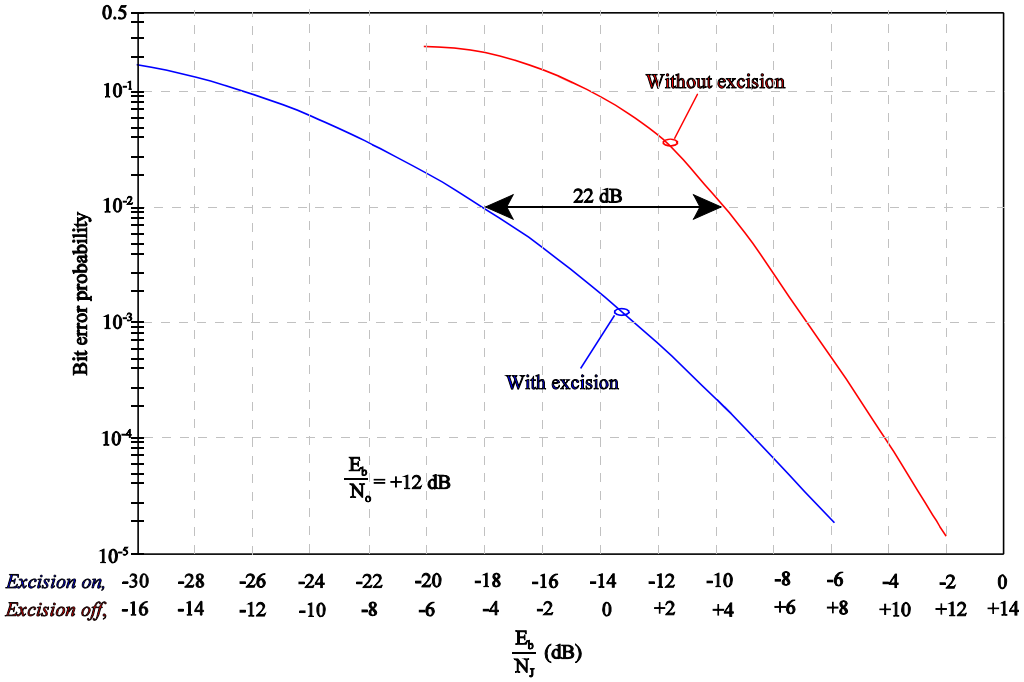

Figure 21 Rectangular window.

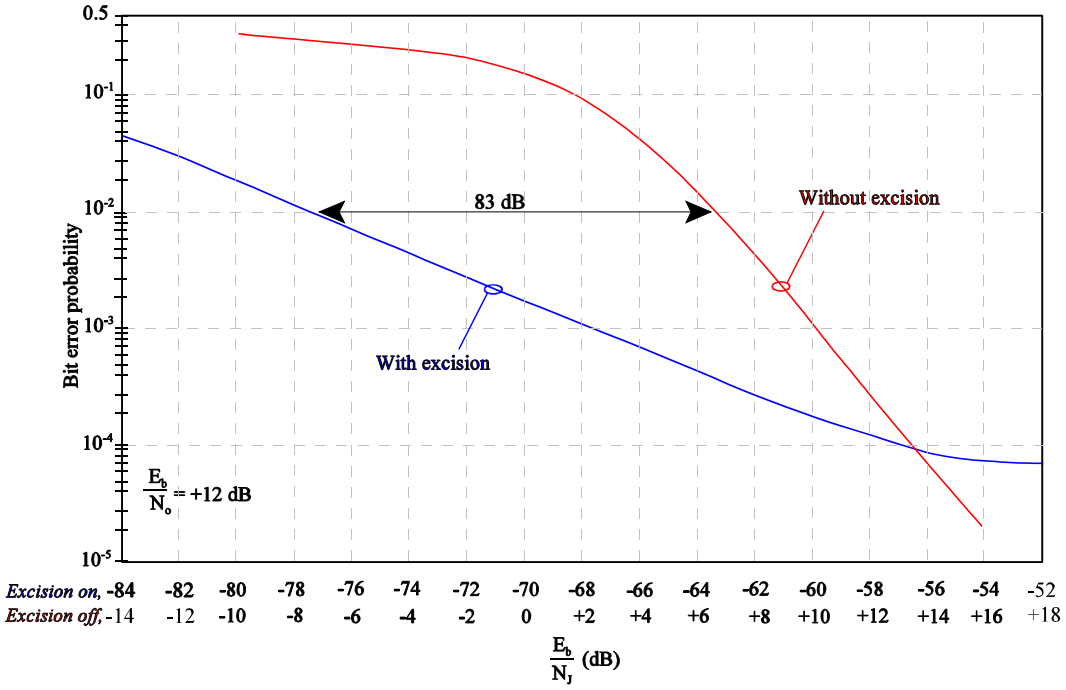

Figure 22 Hanning window.

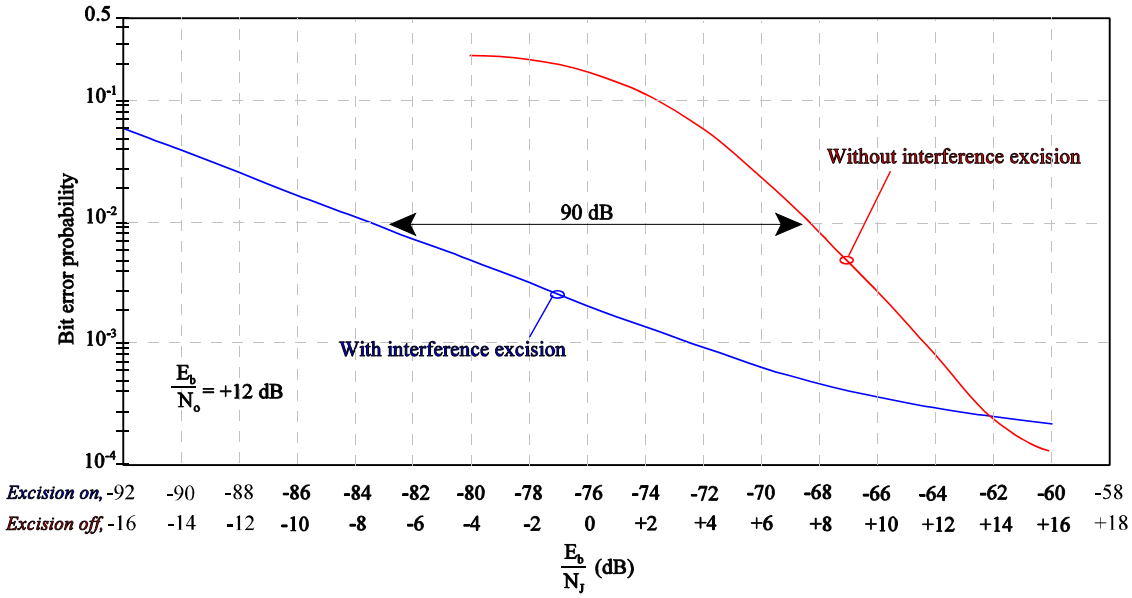

Figure 23 Blackman window.

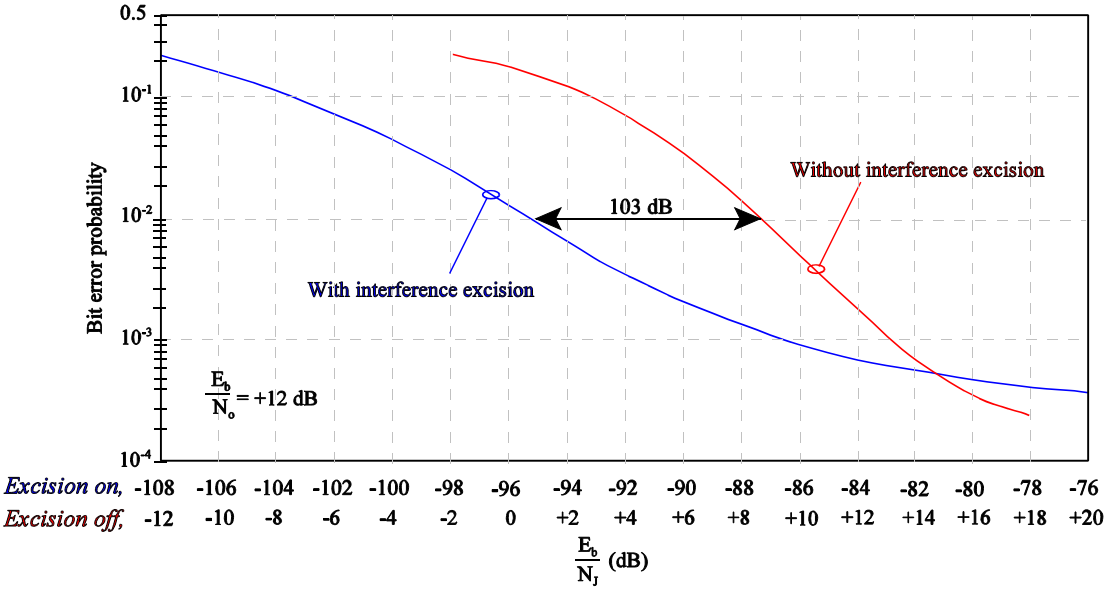

Figure 24 Blackman-Harris window.

Appendix 2

Listing and brief description of simulation programs.

All programs are written in Borland C++ version 5.02, and are compiled to run under a DOS full screen session.

The following two files are required by many of the simulation routines:

timewin.cpp	Time domain window definitions, e.g. Hanning, Blackman, etc.
fft.cpp	Fast Fourier transform and inverse fast Fourier transform routines.

These are included on the attached CD-ROM.

2.1 Programs in support of chapter 2.

i) adapprbs.cpp (Associated project file = adapprbs.ide)
Graphical display of signals within the receiver using a binary pseudo-random spreading function. This program was used in the initial development of the batch files listed below. It is included here because it provides a useful insight into the excision process. The signals shown are:

Received signal + noise + jammer.	(Top trace)
Receiver reference function.	(Middle trace).
Integrate and dump voltage.	(Bottom trace).

The simulation parameters are set at the head of routine 'main' prior to compiling. The included executable version has the following settings:

```
double SNR_dB = 12.0;          /* Signal to AWGN power ratio, in dB. */
double SJR_dB = 40.0;          /* Signal to CW interference power ratio, in dB.*/
float excision =    on;        /* CW excision is 'on' or 'off'. */
float notch_width = 16.0;      /* Width of notch below and above jammer. */
float sweep = on;              /* Jammer frequency is either fixed ('off') or swept ('on'). */
float cw_freq = 22.50;         /* CW jammer start frequency or fixed frequency in bins. */
                               /* Bin 22 => 2.2 kHz, bin 102 => 10 kHz. */
                               /* 1/2 bin offset gives maximum aliasing. */
float step = 1.0;              /* Step increment for swept jammer, in bin numbers. */
float graph = on;              /* graph plot is 'on' or 'off' */
float gain1 = 3.0;             /* Trace gains for plot routine. */
float gain2 = 10.0;            /* gain1 is top trace, gain2 is middle trace, */
float gain3 = 0.03;            /* gain3 is bottom trace.  */
int winnum = 1;                /* Window type, 1 = rectangular, 2 = Hamming, 3 = Hanning,
                               4 = Triangular, 5 = Blackman, 6 = Blackman-Harris. */
```

ii) batprbs.cpp (Associated project file = batprbs.ide)
Batch file for simulating adaptive system with binary pseudo-random spreading function. The routine is modified as required for stepping the parameter under investigation, e.g. notch width, SJR, etc. Results are written to files for inspection under Windows Notepad.

iii) adaprand.cpp (Associated project file = adaprand.ide)
Graphical display of signals within the receiver using a random phase spreading function. The signals shown are:

Received signal + noise + jammer.	(Top trace)
Receiver reference function.	(Middle trace).
Integrate and dump voltage.	(Bottom trace).

The simulation parameters are set at the head of routine 'main' prior to compiling. The included executable version has the following settings:

```
double SNR_dB = 12.0;          /* Signal to AWGN power ratio, in dB. */
double SJR_dB = 40.0;          /* Signal to CW interference power ratio, in dB.*/
float excision = on;           /* CW excision is 'on' or 'off'. */
float notch_width = 16.0;      /* Width of notch below and above jammer. */
float sweep = on;              /* Jammer frequency is either fixed ('off') or swept ('on'). */
float cw_freq = 22.50;         /* CW jammer start frequency or fixed frequency in bins. */
                               /* Bin 22 => 2.2 kHz, bin 102 => 10 kHz. */
                               /* 1/2 bin offset gives maximum aliasing. */
float step = 1.0;              /* Step increment for swept jammer, in bin numbers. */
float graph = on;              /* graph plot is 'on' or 'off' */
float gain1 = 40.0;            /* Trace gains for plot routine. */
float gain2 = 600.0;           /* gain1 is top trace, gain2 is middle trace, */
float gain3 = 100.0;           /* gain3 is bottom trace.  */
int winnum = 1;                /* Window type, 1 = rectangular, 2 = Hamming, 3 = Hanning,
                               4 = Triangular, 5 = Blackman, 6 = Blackman-Harris. */
```

iv) batrand.cpp (Associated project file = batrand.ide)
Batch file for simulating adaptive system with random phase spreading function. The routine is modified as required for stepping the parameter under investigation, e.g. notch width, SJR, etc. Results are written to files for inspection under Windows Notepad.

2.2 Programs in support of chapter 5.

i) pnd&mdet.cpp (Associated project file = pnd&mdet.ide)
Graphical display of signals within an ESM receiver using the delay and multiply technique, when receiving a direct sequence signal using a binary pseudo-random spreading function. The signals shown are:

Received signal + noise.	(Top trace)
Power spectrum of received signal.	(Middle trace).
FFT of delay and multiply output.	(Bottom trace).

The receiver's estimate of the direct sequence carrier frequency is shown by the red circle on the power spectrum trace.

Simulation parameters may be changed using function keys as displayed at the top of the screen.

ii) batd&mpn.cpp (Associated project file = batd&mpn.ide)
Batch file for delay and multiply receiver and binary PN function. The routine is modified as required for stepping the parameter under investigation. Results are written to files for inspection under Windows Notepad.

iii) rdd&mdet.cpp (Associated project file = rdd&mdet.ide)
Graphical display of signals within an ESM receiver using the delay and multiply technique, when receiving a direct sequence signal using a random phase spreading function.
The signals shown are:

Received signal + noise.	(Top trace)
Power spectrum of received signal.	(Middle trace).
FFT of delay and multiply output.	(Bottom trace).

The receiver's estimate of the direct sequence carrier frequency is shown by the red circle on the power spectrum trace.

Simulation parameters may be changed using function keys as displayed at the top of the screen.

iv) batd&mrd.cpp (Associated project file = batd&mrd.ide)
Batch file for delay and multiply receiver and random phase function. The routine is modified as required for stepping the parameter under investigation. Results are written to files for inspection under Windows Notepad.

v) pncordet.cpp (Associated project file = pncordet.ide)
Graphical display of signals within an ESM receiver using the sideband correlation technique, when receiving a direct sequence signal using a binary pseudo-random spreading function.
The signals shown are:

Received signal + noise.	(Top trace)
Power spectrum of received signal.	(Middle trace).
Correlation result.	(Bottom trace).

The receiver's estimate of the direct sequence carrier frequency is shown by the red circle on the power spectrum trace.

Simulation parameters may be changed using function keys as displayed at the top of the screen. The size of the averaging window (shown as alpha) is a function of signal to noise ratio, and is calculated using equation 6 in section 5.3.

vi) batdetpn.cpp (Associated project file = batdetpn.ide)
Batch file for sideband correlation receiver and binary pseudo-random function. The routine is modified as required for stepping the parameter under investigation. Results are written to files for inspection under Windows Notepad.

vii) rdcordet.cpp (Associated project file = rdcordet.ide)
Graphical display of signals within an ESM receiver using the sideband correlation technique, when receiving a direct sequence signal using a random phase spreading function.
The signals shown are:

Received signal + noise.	(Top trace)
Power spectrum of received signal.	(Middle trace).
Correlation result.	(Bottom trace).

The receiver's estimate of the direct sequence carrier frequency is shown by the red circle on the power spectrum trace.

Simulation parameters may be changed using function keys as displayed at the top of the screen. The size of the averaging window (shown as alpha) is not a function of SNR and is fixed at 64.

viii) batdetrd.cpp (Associated project file = batdetrd.ide)
Batch file for sideband correlation receiver and random phase function. The routine is modified as required for stepping the parameter under investigation. Results are written to files for inspection under Windows Notepad.